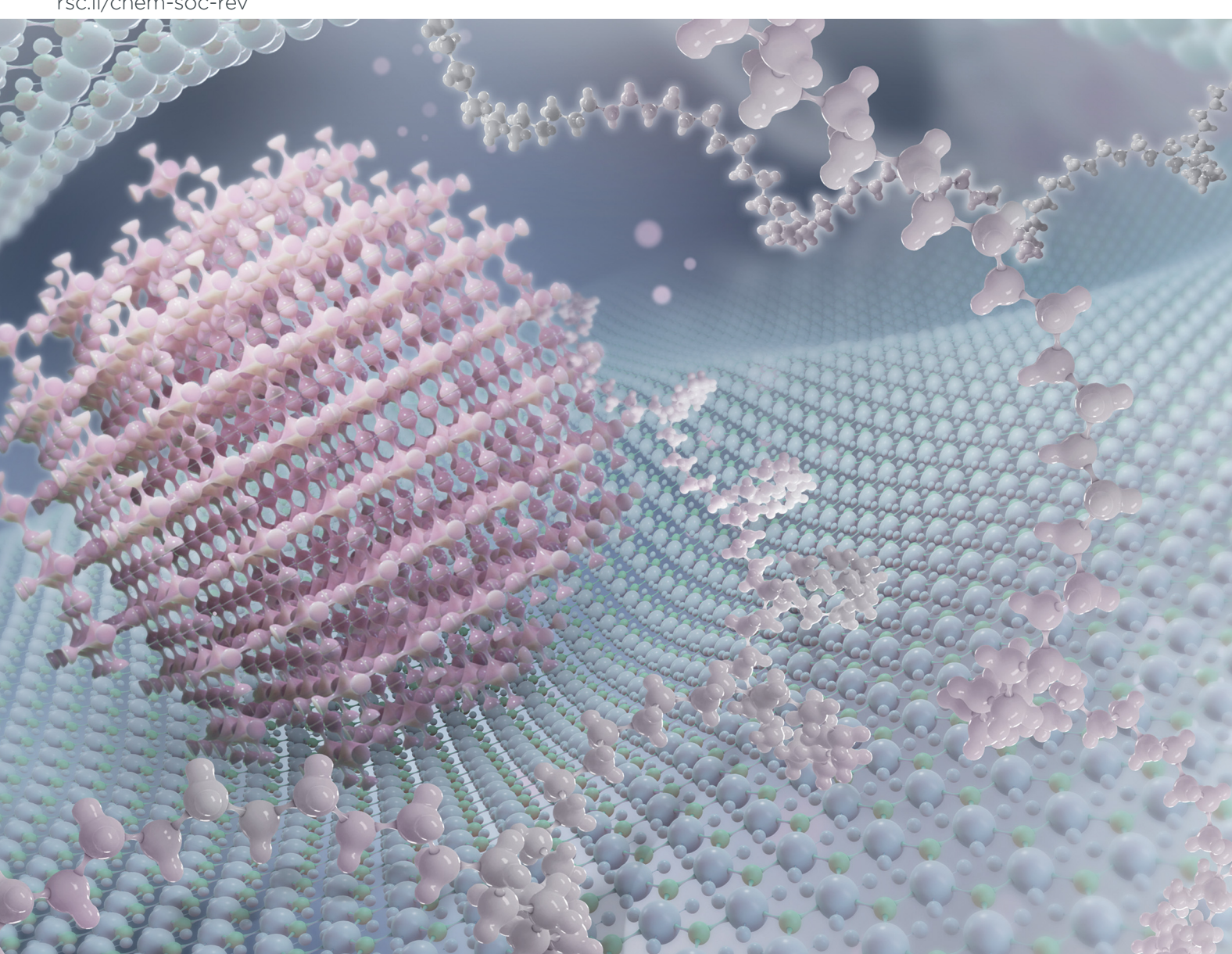
Volume 52 Number 23 7 December 2023 Pages 8079-8448

Chem Soc Rev

Chemical Society Reviews

rsc.li/chem-soc-rev



ISSN 0306-0012



Chem Soc Rev



REVIEW ARTICLE

View Article Online



Cite this: Chem. Soc. Rev., 2023, **52**, 8165

3D architectures

Single-crystal polymers (SCPs): from 1D to

Mingsen Wang, Yinghua Jin, Db Wei Zhang b* and Yingjie Zhao b*

Single-crystal polymers (SCPs) with unambiguous chemical structures at atomic-level resolutions have attracted great attention. Obtaining precise structural information of these materials is critical as it enables a deeper understanding of the potential driving forces for specific packing and long-range order, secondary interactions, and kinetic and thermodynamic factors. Such information can ultimately lead to success in controlling the synthesis or engineering of their crystal structures for targeted applications, which could have far-reaching impact. Successful synthesis of SCPs with atomic level control of the structures, especially for those with 2D and 3D architectures, is rare. In this review, we summarize the recent progress in the synthesis of SCPs, including 1D, 2D, and 3D architectures. Solution synthesis, topochemical synthesis, and extreme condition synthesis are summarized and compared. Around 70 examples of SCPs with unambiguous structure information are presented, and their synthesis methods and structural analysis are discussed. This review offers critical insights into the structure-property relationships, providing guidance for the future rational design and bottom-up synthesis of a variety of highly ordered polymers with unprecedented functions and properties.

Received 14th July 2023 DOI: 10.1039/d3cs00553d

rsc li/chem-soc-rev

1 Introduction

Since Staudinger proposed the definition of macromolecules in the early 1920s, ^{1,2} traditional linear polymers (one-dimensional (1D) polymers) have been studied extensively in the past century. In 2004, the successful exfoliation of a graphene monolayer from graphite expanded the structure of traditional linear (1D) polymers to two-dimensional (2D) networks, 3 ushering in the "2D" era. In 2005, Yaghi and co-workers synthesized the first example

of 2D covalent organic frameworks (COFs) through a facile solution synthesis. 4 Subsequently, the first example of 3D COFs was reported by the Yaghi group in 2007.5 Since then, diversified polymeric structures with complex 2D and 3D topologies have been achieved through deliberate control and manipulation of the building blocks and synthetic conditions.^{6,7} Despite the great advances in this field, there is still no straightforward method for preparing large single crystals of these 2D and 3D polymeric architectures with complete structural control, analogous to how nature creates 2D graphite or 3D diamond. Usually, polycrystalline powders are obtained through the kinetic polymerization process under solvothermal conditions.8 The precise control of the polymerization in 2D or 3D spaces to obtain large-sized 2D or 3D single-crystal polymers (SCPs) has been a very challenging

^b Department of Chemistry, University of Colorado Boulder, Boulder, Colorado 80309, USA. E-mail: wei.zhang@colorado.edu



Mingsen Wang

Mingsen Wang received his BS degree from Qingdao University of Science and Technology in 2020. He is currently studying for his MS degree under the supervision of Prof. Yingjie Zhao at Qingdao University of Science and Technology. His research interests are porous organic materials.



Yinghua Jin

Yinghua (Alice) Jin received her BS Chemistry from Peking University in 2000. She obtained her PhD in Chemistry under the supervision of Prof. Robert M. Coates from the University of Illinois at Urbana-Champaign (UIUC) in 2006. Her research interests include the development of novel organic functional materials and their applications in energy and biomedical fields.

^a College of Polymer Science and Engineering, Qingdao University of Science and Technology, Qingdao 266000, China. E-mail: yz@qust.edu.cn

task. In 2014, the first example of large-sized 2D SCPs was successfully prepared by Schlüter and co-workers through topochemical polymerization.9 A breakthrough in the synthesis of large-sized single-crystal 3D COFs from solution was realized by Wuest, Wang, and Yaghi. 10,11 The single-crystal polymeric structures with atomic resolution is critical in understanding many fundamental questions. For example, how can we achieve long-range order through the packing and secondary interactions of 1D polymer chains? What are the exact stacking modes of the layers in 2D COFs along the c-axis direction? What are the exact interpenetrations in 3D COFs that are usually hard for the common powder X-ray diffraction (PXRD) to determine?^{6,8,12-14} What is the arrangement of the guest molecules within the framework?¹¹ etc. There are still many unknowns in polymeric architectures, which have strongly impeded their structure-property relationship study, mechanism understanding, the exploration of structure-oriented applications, and the development of next-generation functional materials.

In this review, we summarize the recent development in the controlled synthesis of SCPs. We focus on the single crystals of 1D, 2D and 3D covalently linked polymers. The chosen examples of the SCPs discussed here should have unambiguous structures determined by either a single-crystal X-ray diffraction (SCXRD) or electron diffraction technique, 14-16 which could give clear atomic-level structure information. The examples of SCPs are classified into 1D, 2D, and 3D architectures, which were further categorized based on the different synthetic strategies into solution synthesis, topochemical synthesis, and others (Fig. 1). Finally, the review concludes with perspectives on the current problems, possible solutions, and future endeavors, providing valuable perspectives in the field of SCPs.

2 1D architectures

2.1 Recrystallization

1D polymers, also known as linear polymers, have been a topic of research for more than 100 years. Due to the good solubility of most 1D polymers, the growth of single crystals could be realized by a recrystallization process similar to the case of small molecules. 17-20 Even so, compared to small molecules, the reported single crystals of 1D polymers with unambiguous atom-level structure information are still rare. 21-25 Significant research efforts have been devoted to the controlled synthesis of 1D SCPs. 26-29

High-quality single crystals of 1D polymer are not easily available or accessible because high molecular weight 1D polymers often form powders or spherulitic films when they are crystalline. In 2003, Henderson and co-workers successfully obtained a single crystal of 1D-P-1 from a low molecular weight polyethylene oxide (PEO) (Fig. 2a).³⁰ The solution of 1D polymer P(EO)₃(500) and LiCF₃SO₃ mixture was kept in a dry room for several weeks to give long needle-like single crystals. The single crystal 1D-P-1 was analyzed by SCXRD, which revealed a monoclinic unit cell with the space group $P2_1/n$. It should be noted that each Li⁺ cation is coordinated with three oxygen atoms from PEO and two oxygen donors from two CF₃SO₃⁻ anions (Fig. 2b). A linear helical chain was formed using the Li⁺ cation as a template. These linear chains are stacked in parallel to form single crystals (Fig. 2c and d).

Bruce and co-workers reported a 1D-P-2 single crystal with sufficient quality for SCXRD (Fig. 2e).31 The single crystal was grown by combining NaAsF6 salt with PEO in acetonitrile, followed by slow evaporation. Experimental and simulated PXRD patterns show excellent agreement, indicating the bulk powder sample has the same crystalline phase as the single crystal. Similar to the structure of 1D-P-1, the SCXRD reveals that Li⁺ cations are coordinated with the oxygen atoms in the polymer chain, leading to the formation of a helical structure (Fig. 2f-h).

2.2 Solution synthesis

While the crystallization of 1D polymer solutions can lead to the formation of SCPs in a relatively easy way, the strategy is highly dependent on the solubility and the molecular weight of



Wei Zhang

Wei Zhang received his BS in Chemistry from Peking University in 2000, and his PhD in Chemistry from University of Illinois at Urbana-Champaign (UIUC) in 2005. After a postdoc stint at MIT, he started his independent career at University of Colorado Boulder in 2008. Currently he is a full professor and serves as the Chair of the Department. His research is focused on utilizing dynamic covalent chemistry to

develop novel organic and hybrid functional materials targeting a broad range of environmental, energy and biological applications.



Yingjie Zhao

Yingjie Zhao obtained his PhD from the Institute of Chemistry, Chinese Academy of Sciences, in 2011. From 2011 to 2016, he carried out post-doctoral research at the University of Geneva and ETH Zürich, successively. In 2016, he joined Qingdao University of Science and Technology to start his independent research and was promoted to Full Professor in the same year. The main research interests of Zhao are crystalline nanoporous materials and supramolecular chemistry.

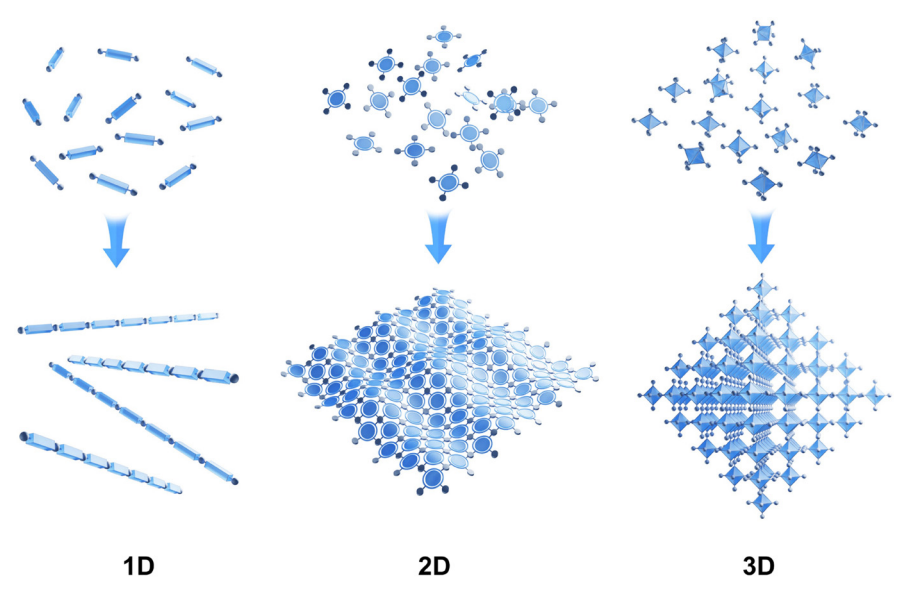


Fig. 1 Schematic diagram of the preparation of 1D, 2D and 3D architectures.

the polymers. As a result, there has been a growing interest in direct synthetic strategies of SCPs in solution. The development of dynamic covalent chemistry has contributed significantly to constructing highly ordered structures, such as COFs, through solution synthesis. 32-43 The self-correction process in dynamic covalent chemistry enables the formation of SCPs with high degrees of structural order. 44-55 Compared to 2D and 3D COFs, the synthesis of lower dimensional 1D COFs in solution has been less reported. The 1D COFs synthesis is hampered by the anisotropy and the entropy-driven random packing of the linear organic chains.56 The high symmetries and limited freedom of the intermolecular packing in 2D or 3D COFs usually facilitate their crystallization process. In 1D COFs, the molecular packing is more flexible because their covalent links are confined to a

single dimension. 56,57 Therefore, external noncovalent interactions, such as hydrogen bonding, hydrophobic interactions, or π - π stacking interactions, are generally needed to form ordered crystalline structures of 1D COFs.

Zhang and co-workers recently reported a 1D helical SCP.⁵⁸ The single-crystalline helical structures through either a hydrogen bond or metal coordination have been reported by Huc, Nitschke, etc. 59-62 In this work, the 1D polymer 1D-P-3 was synthesized through a condensation reaction of 1D-M-1 with 1D-M-2 in the presence of LiOH (Fig. 3a). Large-sized single crystals were formed during the polymerization in a solution (Fig. 3b). Based on the assumption that all three diol groups would be converted into spiroborate linkages, a 2D COF was expected to form by consuming the 1D-M-1 and 1D-M-2 at a

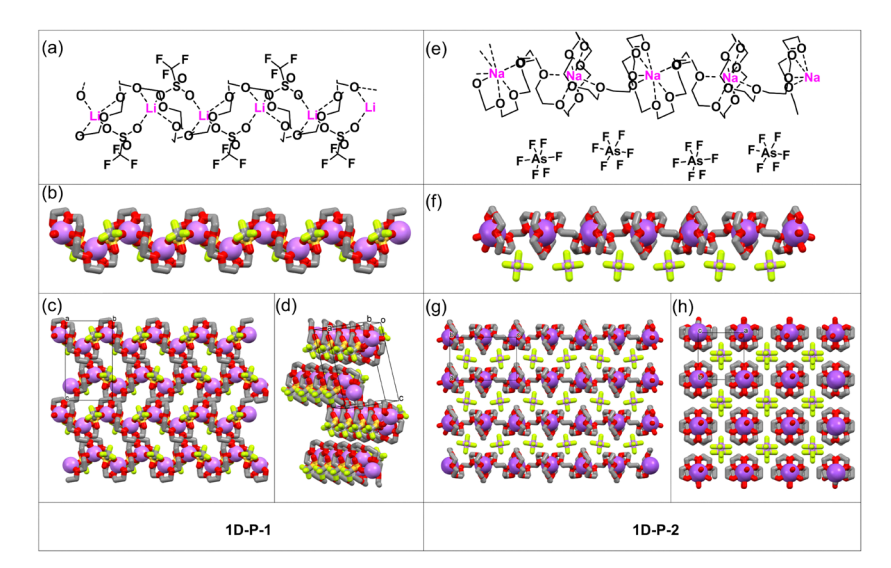


Fig. 2 1D polymer with metal-ligand interactions: (a) the chemical structure of 1D-P-1. (b) The single-crystal structure of a single-chain of 1D-P-1. (c) View of the packing mode along the a-axis. (d) View of the packing mode along the b-axis. (e) The chemical structure of 1D-P-2. (f) The single-crystal structure of a single-chain of 1D-P-2. (g) View of the packing mode along the b-axis. (h) View of the packing mode along the c-axis.

1D-M-2

Review Article

Fig. 3 Helical 1D polymer with hydrogen bonding: (a) synthesis of the 1D helical polymer 1D-P-3; (b) optical images of the large single crystals of 1D-P-3; (c) a stick representation of the strands along the b-axis; (d) formation of helical strands through hydrogen-bonding interactions along the a axis; (e) the view along the a-axis. Reproduced with permission from ref. 58, Copyright 2021, Springer Nature.

ratio of 2:3. Unexpectedly, only two pairs of diols in each 1D-M-1 participated in the reaction, forming 1D zigzag-shaped polymer chains (Fig. 3a and c). The hydrogen bond interactions between the spiroborate units and the unreacted diols provide the energy gain and stabilization, which led to the formation of the unusual helical backbone (Fig. 3d). Notably, the helical strands form double helices not through strong noncovalent interactions between the two strands of the same pair but through the hydrogen bonding interactions with the strand of a neighboring helical pair (mechanically entwined) (Fig. 3e). This is very different from DNA and most of the reported synthetic doublehelical polymers in which the pair of strands are usually packed together through the noncovalent interactions within the pair.

In addition to hydrogen bonding interactions, metal-ligand interactions have also been found critical in forming 1D SCP structures with structural order. Loh and co-workers combined the reversibility of metal coordination bonds and dynamic covalent bonds to prepare the 1D covalent SCPs (1D-P-4). 56 As shown in Fig. 4a, the polymerization of the two monomers 1D-M-3 and 1D-M-4 led to the poorly crystalline 1D conjugated polymer. Notably, when a suitable amount of AgBF4 was introduced, self-assembly of the linear polymer chains via coordination occurred, yielding micrometer-sized 1D metallo-COF single crystals (1D-P-4) (Fig. 4b). Single-crystal electron diffraction (SCED) with a resolution of ~ 0.95 Å shows a zigzag packing mode (Fig. 4c). Moreover, further polymerization in the crystalline state led to the formation of a 3D woven network while preserving the original polymer backbone (Fig. 4d).

The same group subsequently reported a similar example in which copper ions were used instead of silver ions (Fig. 5a).⁶³ The polymerization of a homoleptic complex 1D-M-5 and a polydentate linker 1D-M-4 produced a heteroleptic species through ligand exchange, resulting in the formation of a 1D COF (1D-P-5) (Fig. 5a). The structure of the obtained 1D-P-5 was confirmed by PXRD and three-dimensional electron diffraction analysis (3D ED). In 1D-P-5, 1D-M-3 molecules are arranged orderly along the conjugated zigzag backbones formed by imine-linked phenanthroline (Fig. 5b).

These studies have demonstrated that the combined use of metal coordination and dynamic covalent chemistry could broaden the scope of COF synthesis. Most importantly, the introduction of metal coordination facilitates the growth of single crystals of 1D COFs. Besides 1D structures, this strategy has also been successfully used in the construction of 3D COF single crystals. A detailed discussion of the 3D metal woven COFs will be presented in the later section on 3D architectures.

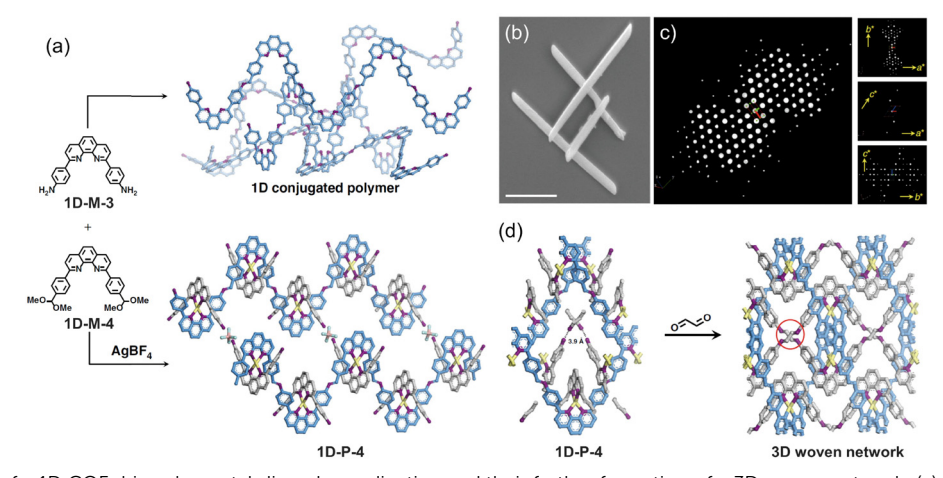


Fig. 4 Crystallization of a 1D COF driven by metal-ligand coordination and their further formation of a 3D woven network: (a) schematic illustration of 1D metallo-COF synthesis; (b) SEM image of 1D-P-4; (c) the lattice of 1D-P-4 reconstructed from the SCED data; (d) crystalline-state polymerization process. Reproduced with permission from ref. 56, Copyright 2020, Springer Nature.

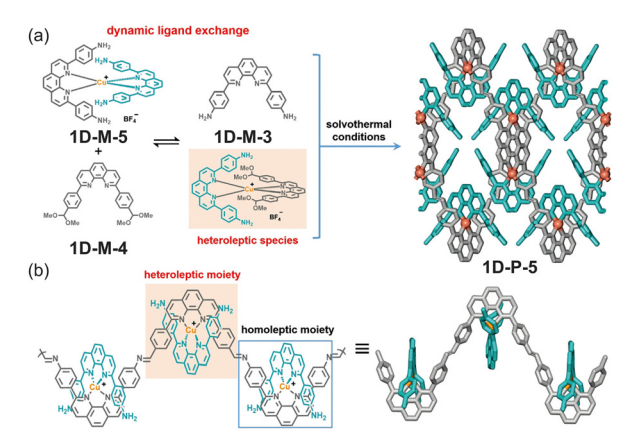


Fig. 5 Formation of 1D COF through dynamic ligand exchange: (a) synthesis of 1D-P-5 and the chemical composition of a single zigzag chain; (b) strategies for constructing 1D-P-5. Reproduced with permission from ref. 63, Copyright 2020, Wiley-VCH.

Topochemical polymerization

Topochemical reactions in a single-crystal state have been a hot subject of investigation for several decades.⁶⁴⁻⁶⁸ The topochemical polymerization approach allows the preparation of SCPs from pre-assembled monomer crystals through a single-crystalto-single-crystal (SCSC) transformation. 69-71 Compared to solution-based synthesis, this solid-state synthesis provides a new method for preparing SCPs. However, this approach is highly dependent on the molecular packing within the single crystal of monomers. Although the strict geometric requirements of topochemical polymerizations and the challenges in monomer design have limited the generality of this approach, significant progress has been made. Various reaction types have been successfully employed, including [2+2],⁷²⁻⁷⁷ [4+4],^{9,78-81} diene or triene polymerization, 82-84 quinodimethane polymerization, 85,86 acetylenes polymerization^{87–92} and azide–alkyne cycloaddition.^{93–99} The examples of 1D SCPs obtained by SCSC transformation have also been reviewed in several excellent articles. 67,70,100–102

2.3.1 [2+2] photo-dimerization. The pioneering work of crystalline 1D polymers prepared in the solid state by the [2+2] photo-dimerization was reported in 1969 by Hasegawa and coworkers. 103 Since then, [2+2] photo-dimerization has been widely utilized to synthesize 1D SCPs. 104-112 Recently, Stoddart and Guo employed the self-complementary effects of the pyridinium-based system due to their shape and charge distribution interactions and successfully prepared single-crystal polycationic polymers through [2+2] SCSC topochemical photopolymerization.⁷⁷ As shown in Fig. 6, a triolefinic tripyridinium monomer 1D-M-6 was first designed and synthesized, which adopts a conformation wherein two transstyrylpyridinium arms are oriented in one direction, while the third arm is oriented in the opposite direction. Two of three pyridinium arms adopt anti-parallel co-conformations with those in adjacent molecules to form an infinite linear superstructure in which all the neighboring monomers are integrated noncovalently in the crystal. The third arm of the monomer is free and does not form pairs with adjacent monomers. The subsequent irradiation of the monomer single crystals with ultraviolet light (λ = 365 nm) at 100 K for 9 hours resulted in the formation of 1D SCPs (1D-P-6). Subsequently, by using the same strategy, they successfully obtained another example of 1D SCP with very large molecular weights. 113 As shown in Fig. 7a, bipyridinium monomer 1D-M-7 was designed and synthesized, which can self-assemble into an infinite 1D supramolecular structure through anti-parallel co-conformations employing self-complementary interactions between pyridiniumbased appendages. 1D SCP 1D-P-7 was obtained by irradiating the monomer crystals with UV light at 100 K for 6 hours. Notably, 1D-P-7 exhibits good solubility in strong polar solvents, which enables their in-depth characterization in the solution phase.

Biradha and co-workers reported two examples of 1D SCPs through [2+2] photo-dimerization in single-crystal states.⁷⁵ As shown in Fig. 7b and c, 1D-M-8 and 1D-M-9 with similar structures were designed to contain bisamide groups. The potential hydrogen bond-induced secondary structures can promote the [2+2] photo-dimerization. 1D-M-8 and 1D-M-9 adopt 1D alignment of molecules along the a-axis arranged through π - π interactions between the amide and phenyl or pyridyl groups. Irradiation of the single crystals of 1D-M-8 and 1D-M-9 under sunlight for 22 hours results in the [2+2] reaction occurring in an SCSC manner to yield single crystals of the 1D-P-8 and 1D-P-9. The strong hydrogen-bonding interactions of the bisamide groups induced 2D layered structures, which also promoted the [2+2] polymerization reaction.

2.3.2 [4+4] photo-dimerization. Schlüter and Servalli reported a novel ladder-type 1D SCP example through the

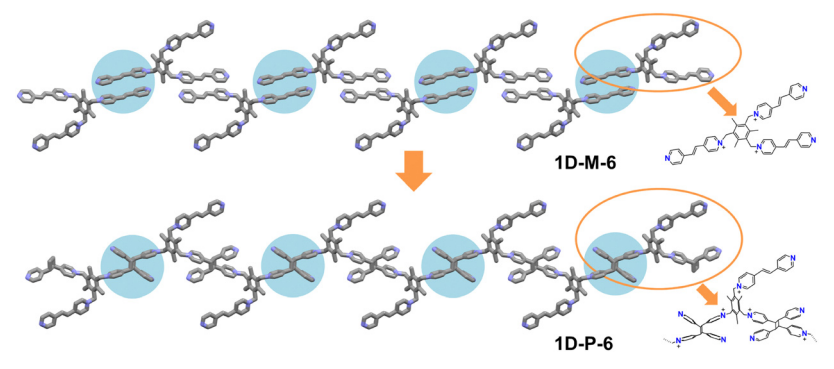


Fig. 6 The single-crystal X-ray structures of 1D-M-6 and 1D-P-6

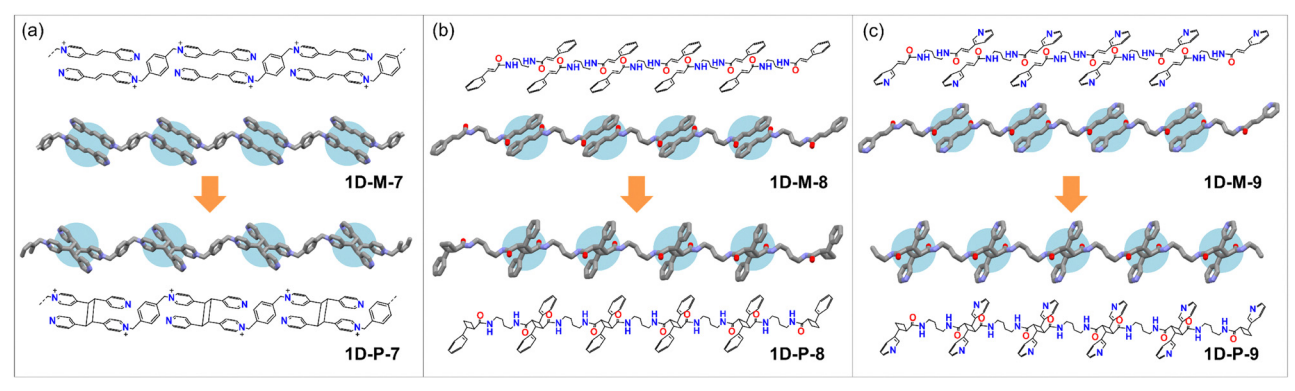


Fig. 7 The chemical and single-crystal X-ray structures of (a) 1D-M-7 and 1D-P-7; (b) 1D-M-8 and 1D-P-8; (c) 1D-M-9 and 1D-P-9

[4+4] photo-dimerization of the anthracene-based monomer.⁷⁹ A desymmetrized anthracene-based monomer 1D-M-10 was designed with methoxy substituents to break the symmetry (Fig. 8a). Each 1D-M-10 molecule has two anthracene units face-to-face stacking with the anthracene units of its neighbors, leading to potential 1D polymer chains upon photoreaction. The photopolymerization in the single-crystal state was realized by the 15 min irradiation under 465 nm UV light. Monomer single crystals 1D-M-10 smoothly convert into polymer single crystals 1D-P-10. Zhang and co-workers reported an example of platinum-based 1D SCP through the [4+4] cycloaddition of anthracene in an SCSC fashion.⁷⁸ They employ a platinum coordination-driven self-assembly strategy to secure the appropriate head-to-tail alignment of anthracene moieties in monomer 1D-M-11 (Fig. 8b). The coordination-driven force induces an appropriate alignment of the 1D-M-11. The anthracene blades in 1D-M-11 are aligned in a head-to-tail manner with strong π - π stacking between the anthracenes. The subsequent irradiation of the 1D-M-11 single crystals with white light at 265 K for 9 days resulted in the formation of 1D-P-11. Taking advantage of the temperature-dependent slow depolymerization, this Pt-based 1D polymer showed potential as a sustainedrelease anticancer drug platform.

2.3.3 Polymerization of dienes and trienes. The polymerization of 1,3-diene derivatives can also realize the SCSC topochemical reaction. 82,83,114-123 Matsumoto and co-workers reported a 1,3-diene dicarboxylic acid monomer 1D-M-12 with substitution of a chlorine atom in the aromatic hydrogen of the benzyl group (Fig. 9a). 82 The SCXRD revealed that the planar diene moieties are closely packed to form a columnar structure in the crystals. Both weak halogen-halogen and CH/π interactions are important for the self-assembly of 1D-M-12 in an appropriate mode. The photoirradiation was carried out using γ-ray radiation at room temperature, leading to the successful polymerization of 1D-M-12 in a single-crystal state. The topochemical polymerization of 1D-M-12 proceeds with a transformation in the chemical bond with the minimum movement of atoms to produce 1D SCP 1D-P-12. The same group further reported a fluorine-substituted 1D-M-13, which has a similar structure to the chlorine-substituted 1D-M-12 (Fig. 9b). 124 The intermolecular interactions such as C-H···O and C-H···F interactions contribute to the formation of a columnar structure with appropriate molecular packing and thus realize the successful polymerization in the single-crystal state under γ -ray radiation to give 1D SCP 1D-P-13. Interestingly, a dimer is exclusively produced under UV irradiation instead of polymerization. The columnar structure with an appropriate stacking

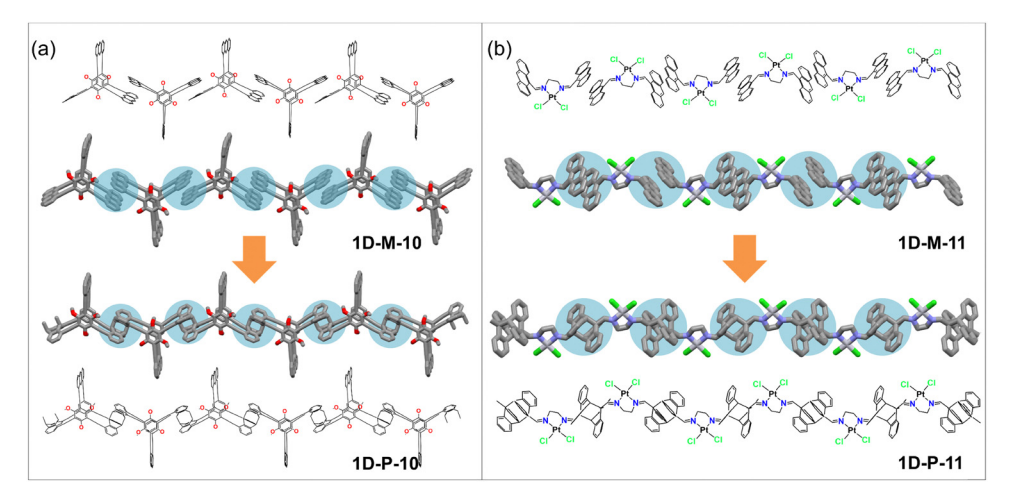


Fig. 8 The chemical and single-crystal X-ray structures of (a) 1D-M-10 and 1D-P-10; (b) 1D-M-11 and 1D-P-11.

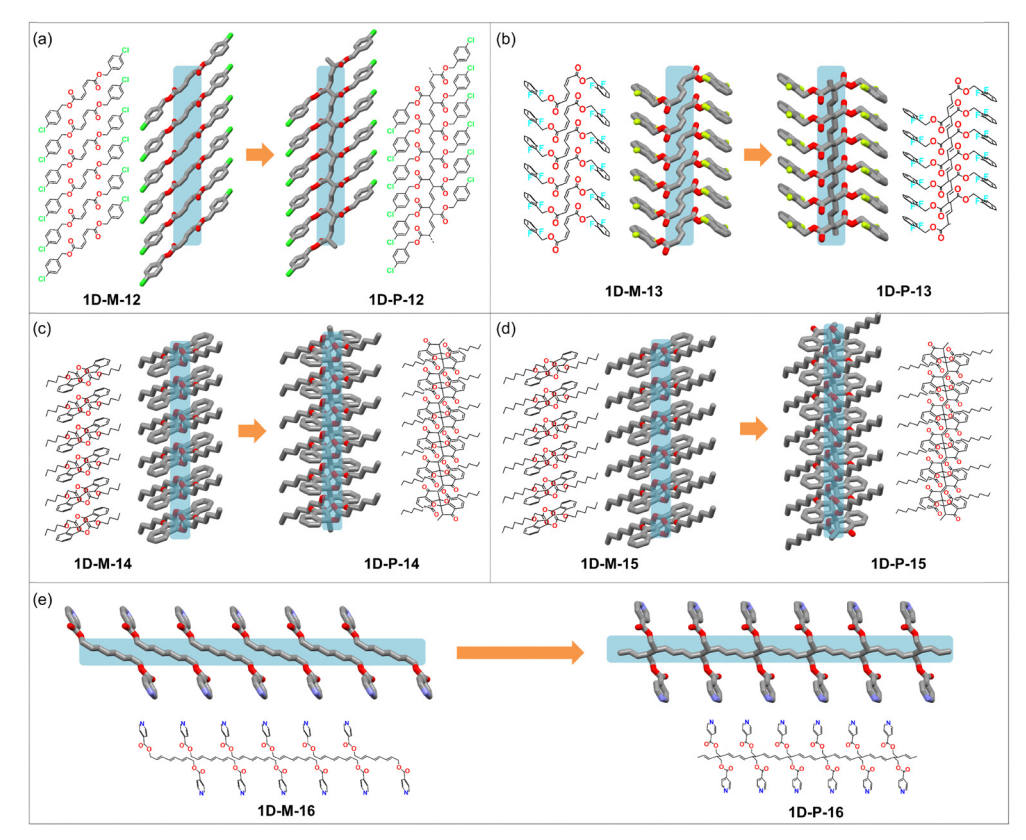


Fig. 9 The chemical and single-crystal X-ray structures of (a) 1D-M-12 and 1D-P-12; (b) 1D-M-13 and 1D-P-13; (c) 1D-M-14 and 1D-P-14; (d) 1D-M-15 and 1D-P-15; (e) 1D-M-16 and 1D-P-16.

distance is indispensable to the successful topochemical polymerization of such 1,3-diene monomers. The too large or small distance is unfavorable for the topochemical polymerization in a single crystal state. 125

Wudl and co-workers realized the visible light-triggered topochemical polymerization reaction of two bi-indene-dione derivatives (1D-M-14 and 1D-M-15) in a single crystal state under sunlight or a high-pressure sodium lamp (Fig. 9c and d). 126

Polymerization is not limited to single crystals but can also be achieved in highly concentrated solutions or semicrystalline thin films. The alkyl side chains in the monomer structures are found to play an important role in molecular packing. The perfect alignment of the monomers in the crystals and the short distance of the two active carbon atoms (~ 3.2 to ~ 3.3 Å) are necessary to ensure the occurrence of the topochemical reactions.

Besides the topochemical 1,3-polymerization of a diene, the 1,6-polymerization of a triene can also realize the transformation in a single crystal state. Lauher and Fowler reported a successful example of topochemical 1,6-polymerization of a triene-based monomer **1D-M-16** (Fig. 9e). ¹²⁷ The π – π stacking of the adjacent pyridine rings in the structures plays a role in determining the stacking modes. The 1-6 carbon-carbon atom distance of adjacent trienes is 4.09 Å, which is a little long for topochemical diene polymerization. However, thermally induced polymerization of 1D-M-16 single crystal resulted in a smooth transformation to 1D-P-16. The X-ray crystal structure determination clearly demonstrated that a topochemical 1,6-polymerization of the triene 1D-M-16 to a polytriene1D-P-16 had occurred (Fig. 9e).

2.3.4 Polymerization of quinodimethane. Itoh and coworkers developed the topochemical polymerization of quinodimethane derivatives. They first realized the copolymerization of 1D-M-17 and 1D-M-18 in the single crystal state (Fig. 10a). 128 An orange-colored single-crystal charge-transfer complex of (1D-M-17 and 1D-M-18) was successfully obtained due to the electron-donating and electron-accepting behavior of these two monomers. The interplanar distance between 1D-M-17 and **1D-M-18** is 3.38 Å, which meets the requirement for the topochemical polymerization. The subsequent UV light irradiation (high-pressure Hg lamp in vacuo for 18 hours) or heating in the dark (60 °C in vacuo for 3 hours) yields colorless or pink alternating copolymer single crystal (1D-P-17) with a cis conformation through successive bond formation between reactive exomethylene carbon atoms.

The same group subsequently reported another example of the quinodimethane-based SCP (Fig. 10b). 86 The yellow platelet monomer single crystals (1D-M-19) can be easily obtained through recrystallization. However, UV irradiation or heating can only lead to low-quality polymer crystal which is not suitable for the SCXRD. The 60 Co γ -radiation with higher energy and better penetration ability was thus utilized for the polymerization in the single-crystal state, which is expected to induce the polymerization rapidly and homogeneously and to provide polymer crystals with fewer defects. After 60Co **Review Article** (a)

Fig. 10 The chemical and single-crystal X-ray structures of (a) 1D-M-17, 1D-M-18 and 1D-P-17; (b) 1D-M-19 and 1D-P-18

1D-P-17

 γ -radiation of 5 kGy at 30 °C for 1 week, the yellow platelet monomer single crystals (1D-M-19) were converted into crackfree colorless, transparent polymer single crystals (1D-P-18). The SCXRD reveals that the monomer molecule forms a columnar structure, and the polymerization takes place along this column structure, where almost no large displacement of the center of mass is observed before and after the polymerization (Fig. 10b).

1D-M-18

2.3.5 Polymerization of diacetylenes and triacetylene. In 1969, Wegner discovered the topochemically controlled 1,4-polymerization of diacetylenes by heating or photo-irradiation. ¹²⁹ Subsequently, Wegner and Baughman elaborated that the appropriate arrangement of the diyne monomers could control their reactivity, leading to ordered topochemical polymerization.²¹ However, in most cases, the divne monomers do not align properly for 1,4polymerization on their own. The key factor thus becomes how to control the appropriate alignment of the monomers in the solid state at a distance commensurate with the repeat distance in the target polymer. The solution to this problem could be found in the field of supramolecular chemistry. 129-139 The weak supramolecular interactions become an ideal choice for the modulation of the monomers' self-assembly. 88,140-149 Goroff and co-workers prepared single-crystal poly(diiododiacetylene) (1D-P-19), a nearly unadorned carbon chain substituted with only single-atom iodine side groups by using a co-crystal scaffolding strategy (Fig. 11a). 150 A Lewis-base bis(nitrile) oxalamide was used as a host to form co-crystals with the monomer diiodobutadiyne (1D-M-20). An appropriate arrangement was successfully acquired through the hydrogen-bonding interactions between the oxalamide groups and weak halogen-bonding interactions between nitriles and iodoalkynes. In the co-crystals with oxalamide as the host, the 1D-M-20 undergoes spontaneous topochemical polymerization to form 1D-P-19 through an SCSC conversion.

1D-M-19

Flowler and Lauher reported 1,6-polymerization of a triacetylene monomer (1D-M-21) in a single crystal state through a host-guest co-crystal strategy. 90 As shown in Fig. 11b, a pyridinebased host and carboxylic acid-based triacetylene as the monomer were co-crystallized to form a 2:1 complex. The hydrogenbonding interactions between the carboxylic acid groups from the monomers and the pyridines from the host molecules realize the approximate arrangement of 1D-M-21 with a reasonable

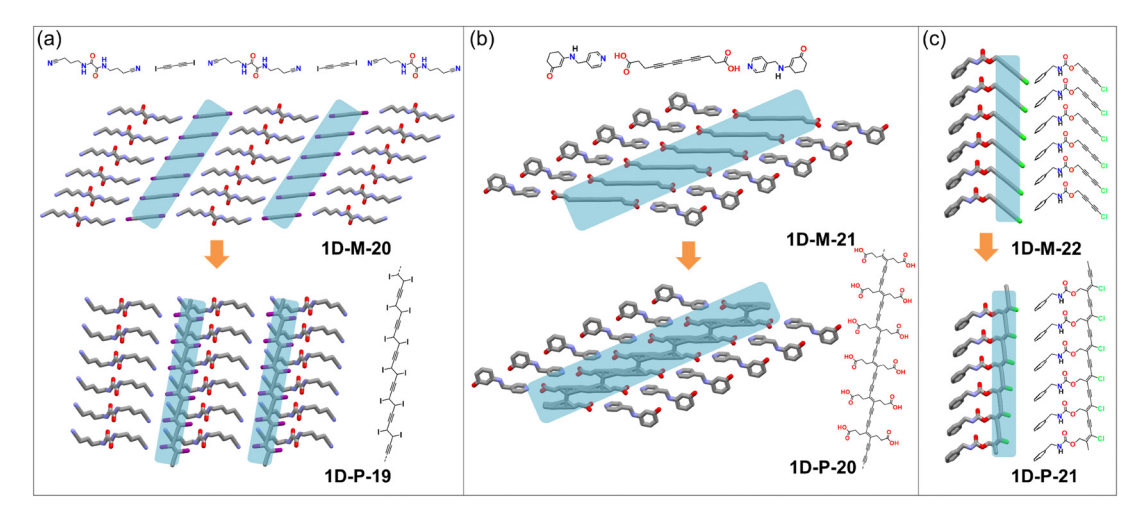


Fig. 11 The chemical and single-crystal X-ray structures of (a) 1D-M-20 and 1D-P-19; (b) 1D-M-21 and 1D-P-20; (c) 1D-M-22 and 1D-P-21.

reactive distance. The subsequent γ -radiation resulted in 70% completion of the polymerization. The further irradiation brings a sudden phase change in the crystals to an amorphous state.

Besides the additional introduction of the host molecules for the regulation of the monomer alignment, the self-assembly of the monomers themselves can also realize an ideal stacking arrangement through the various supramolecular interactions. 129-142 Baillargeon and co-workers reported a topochemical polymerization of chlorodiacetylene (1D-M-22) to afford SCXRD structure determination of polychlorodiacetylene (1D-P-21) (Fig. 11c).⁸⁹ The amide groups in the monomers provide the intermolecular hydrogen bonding interactions of 1D-M-22 for the appropriate alignment of the monomers, thus leading to successful polymerization.

The topochemical polymerization of diacetylenes or triacetylene can lead to 1D conjugated organic polymers, which may exhibit intriguing electronic and optical properties. The unique advantage of this reaction shows great potential in preparing electronic devices, which cannot be realized through other types of topochemical polymerizations. It is worth noting that the preparation of the poly-diyne through topochemical polymerization usually needs a higher energy source. In some cases, γ-radiation is necessary.

2.3.6 Topochemical azide-alkyne and azide-ene cycloadditions. Topochemical reactions have shown significant advantages in the formation of products in an ordered (crystalline) form. However, reactions that can be done topochemically, especially in a single crystal state, are still limited. Sureshan and co-workers developed topochemical azide-alkyne and azide-ene cycloaddition reactions, which can realize the SCSC transformation process.

The azide and alkyne or ene groups in the monomers can undergo 1,3-dipolar cycloaddition in the crystal lattice to yield 1,4- or 1,5-disubstituted 1,2,3-triazole or triazoline products. Triazole or triazoline-linked 1D SCPs were thus formed. Around 13 examples of 1D SCPs have been successfully obtained through these topochemical cycloadditions. We have summarized most of these 1D SCPs examples in Fig. 12, including the chemical structures of monomers and polymers and the transformation process in the single-crystal state. 93,95-98,151-158 In general, hydrogen-bonding interactions, such as O-H···O, N-H···O, and N-H···N, are the main noncovalent driving force for aligning azide and alkyne or ene-substituted derivatives in orientations suitable for their proximity-driven cycloaddition reaction in crystals. The arrangement of azide and alkyne or ene carbohydrates (1D-P-22, 29, 30), nucleosides (1D-P-23), and peptides (1D-P-24, 25, 26, 27, 28, 31, 32, 33, 34) have been successfully exploited for their topochemical azide-alkyne and azide-ene cycloadditions. Thermal activation is the main driving force for the topochemical cycloadditions. Depending on the activation barrier in each case, the cycloaddition reaction can happen spontaneously at room temperature (or even at lower temperatures) or necessitate heating of the single crystals.

In summary, the "click" reaction has shown widespread adoption in various scientific and industrial contexts due to its high efficiency, versatility, and robustness. The discovery by Sureshan and co-workers verified that the widely used "click" reaction can also undergo a topochemical process in a single crystal state and provide triazole or triazoline-linked 1D SPC products. This reaction can be implemented in diverse molecular categories and has a high potential to enrich the variety of the 1D SCPs.

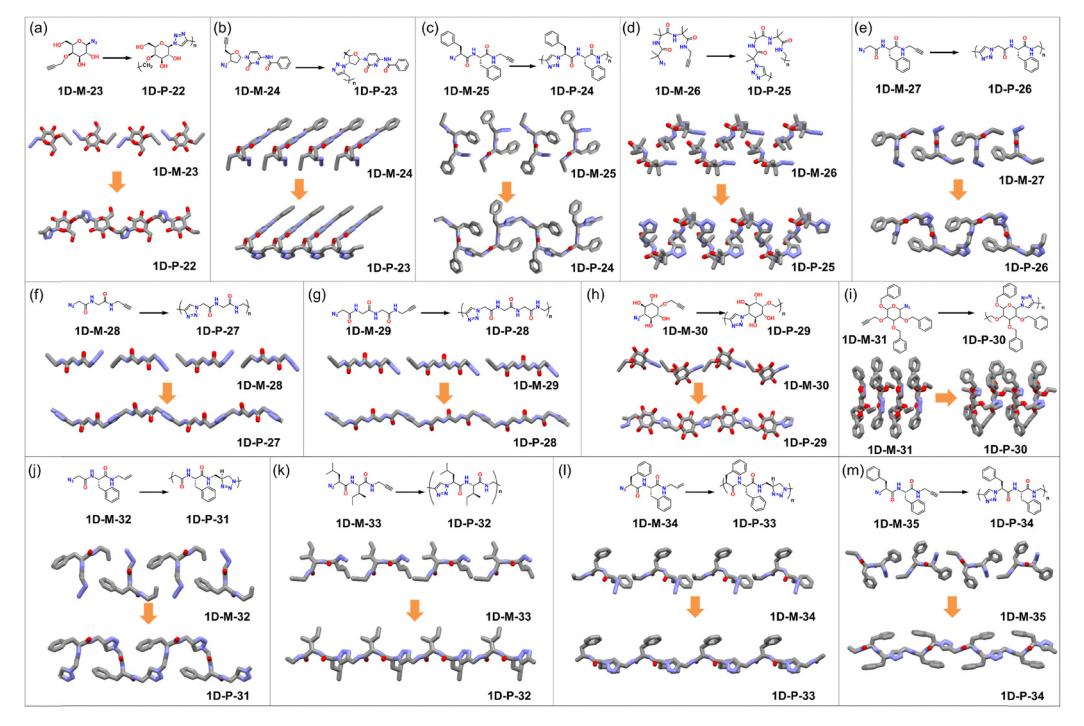


Fig. 12 The chemical and single-crystal X-ray structures of 1D-M-23 to 35 and 1D-P-22 to 34

Review Article

3 2D architectures

The planar nature of 2D architectures can limit their solubilities, making it challenging to obtain single crystals through recrystallization from polymer solutions, as seen in 1D polymer cases. For a long time, researchers have wondered if highly ordered and covalently linked 2D architectures can be made in a laboratory, even though such structures exist in nature, such as crystalline graphite made of 2D graphene layers. Recent advancements in 2D architecture synthesis have shown promising results in the creation of these types of structures. In 2005, the first crystalline 2D COF material was successfully prepared by Yaghi via the solvothermal method in solution.4 This breakthrough discovery has opened up a new era of 2D crystalline polymers, and since then, thousands of 2D COF materials with diverse structures have been designed and synthesized in solution. 5,16,44-46,159 The reversible covalent bond is necessary for the formation of highly ordered structures. Compared to crystalline hydrogen-bonded organic framework (HOF) materials or coordination-bonded metal-organic framework (MOF) materials, COFs are typically more challenging to crystallize. 160-166 Most of the reported COF materials are polycrystalline powders. The structure characterization has been limited to the analysis of PXRD combined with computer simulation modelling. Despite the challenges involved in achieving the atomic-level definitive structures through SCXRD, there have been remarkable breakthroughs in the synthesis of 2D COF single crystals from solutions.

3.1 Solution synthesis

Yaghi and co-workers designed a simple organic linker 2D-M-1 consisting of boronic acid and phosphonic acid groups (Fig. 13a). 167 Through a simple molecular dehydration reaction, a single crystal of 2D layered COFs with a rod unit of an infinite valency structure was obtained, which was referred to as "infinity" (rods) in this study. The single crystals of 2D-P-1 had a block shape (Fig. 13d). The SCXRD structure analysis showed the 1D B-O-P rods consist of alternating tetrahedral boron and phosphorus groups (Fig. 13c and e). These rods were connected by phenylenes, forming a 2D structure with an interlayer spacing of 5.47 Å (Fig. 13b). The layers were stacked along the a axis and arranged in a honeycomb pattern.

Generally, 2D COFs have been obtained as polycrystalline solids with a small crystalline domain size. This could be attributed to the poor control of the nucleation process. Currently, the formation mechanism of 2D COFs remains poorly understood, and the influence of the reaction rates and defect repair process is still largely unknown. Dichtel and co-workers have conducted mechanistic studies on the boronate esterlinked 2D COFs. 168 They found that the nucleation-elongation process was crucial for the growth of the single-crystal COFs (Fig. 14). However, this process is usually disturbed by the precipitation and aggregation of COF microcrystals. A two-step approach is adopted that separates the nucleation and growth processes. A second growth step in which additional monomers were introduced slowly suppressed the further nucleation. The COF colloids can be enlarged into faceted single crystals with

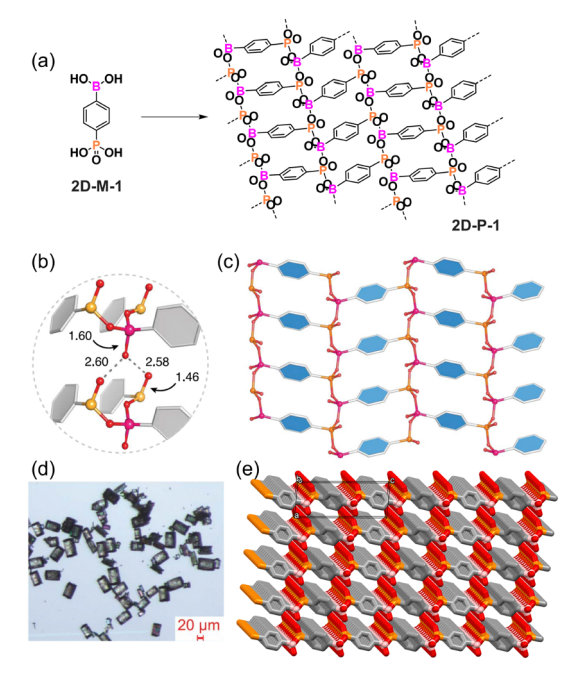


Fig. 13 Solution-based synthesis of single-crystal 2D COFs. (a) The synthesis of 2D-P-1. (b) The H-bonding formation of each layer. (c) Single-crystal X-ray structure of 2D-P-1 in one layer. (d) Optical microscope image of 2D-P-1. (e) The packing mode of 2D-P-1 in a single crystal. Reproduced with permission from ref. 167, Copyright 2020, American Association for the Advancement of Science.

lateral dimensions greater than 1.5 µm. Preventing premature precipitation and aggregation of the microcrystalline COF could help stabilize the colloidal suspensions of single-crystalline boronate ester- and boroxine-linked 2D COF nanoparticles, thus improving the crystalline quality of the products. 168

Dichtel and co-workers found that this colloidal suspension method was also applicable to imine-linked COFs. 169 Micronsized single crystals of two 2D COFs (2D-P-2 and 2D-P-3) were successfully synthesized by using a Schiff base reaction within as little as 5 min (Fig. 15a). The nitrile-containing solvent was used with aniline as a monofunctional modulator and benzoic acid as a catalyst. Large crystals, 4 µm-wide squares of 2D-P-2, and 20 µm-sized hexagons of the 2D-P-3 were obtained by varying the crystallization conditions (Fig. 15b-h). Besides the traditional PXRD characterization, continuous rotation electron diffraction (cRED) was used to elucidate the unit cells of

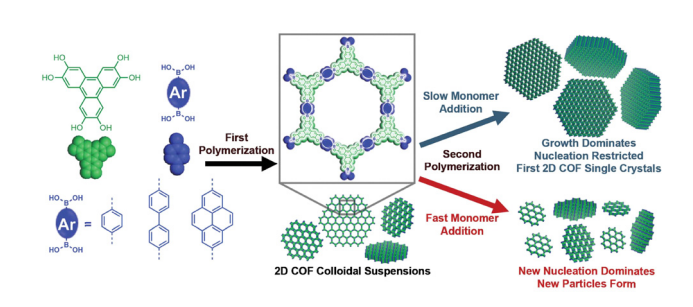


Fig. 14 Schematic of controlled 2D polymerization through a two-step seeded growth approach. Reproduced with permission from ref. 168, Copyright 2018, American Association for the Advancement of Science.

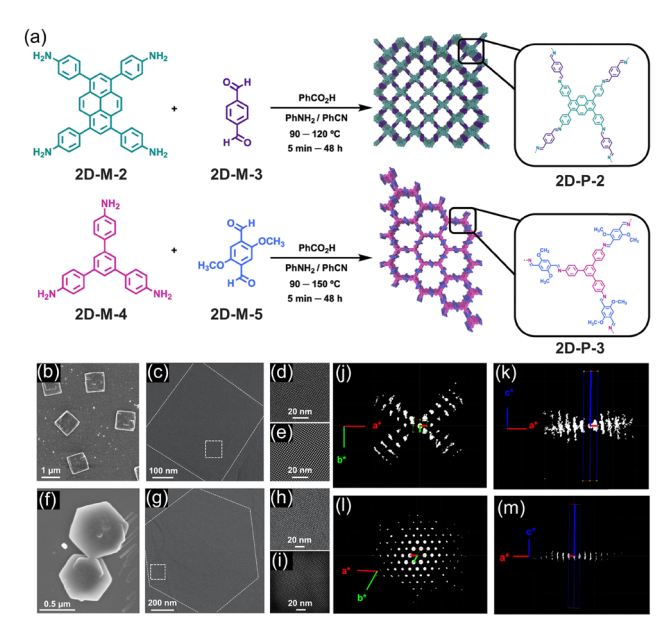


Fig. 15 Solution-based synthesis of single crystal 2D COFs: (a) synthesis of 2D-P-2 and 2D-P-3. (b) SEM and (c)-(e) HRTEM images of 2D-P-2 single crystals. (f) SEM and (g)-(i) HRTEM images of 2D-P-3 single crystals. (j) and (k) 3D reciprocal lattices of the 2D-P-2 at 4.4 Å resolution and (l) and (m) 2D-P-3 at 4 Å resolution, as determined by low-dose cRED. Reproduced with permission from ref. 169, Copyright 2022, American Chemical Society.

2D-P-2 and 2D-P-3 single crystals (Fig. 15j-m). Relatively accurate structure models were obtained by Rietveld refinement. They also proposed that a possible slip-stack happens along the c-axis to minimize the free energy.

Zhao and co-workers obtained a single crystal of 2D COF (2D-P-4) (Fig. 16a), which has identical chemical structure with 2D-P-2.¹⁷⁰ As shown in Fig. 16a, 2D-M-6 was chosen because the aniline-protected aldehyde groups can react with the amine groups of 2D-M-2 at a much lower rate than the unprotected aldehyde groups in 2D-M-7. This provides sufficient time for the pre-arrangement of monomers and oligomers to facilitate crystal growth. Rhombus plate-like single crystals with a size of 2-5 µm were obtained after 30 days of growth (Fig. 16b and c). The authors speculated that the monomers and oligomers go through a self-assembly and pre-arrangement process before the polymerization. Thus, the pyrene-based 2D-M-2 (Fig. 16a) is likely preferred over the benzene core for single crystal growth because the large π -conjugated planar structure would likely enhance inter-molecular binding interactions. The crystal structure of 2D-P-4 was successfully characterized by cRED with a resolution of 0.76 Å (Fig. 16d-f). Interestingly, only 10% of the crystals adopt the widely predicted AA stacking structure (Fig. 16g and h). The remaining 90% of the crystals have a previously unknown stacking structure, containing 6 stacking layers within one unit cell. Unfortunately, this unknown singlecrystal structure could not be resolved due to its high complexity.

Although the above examples of single-crystal 2D COFs reported by the Dichtel and Zhao groups were obtained under different reaction conditions and the research goals are also different, both results indicate the possibility of diverse stacking

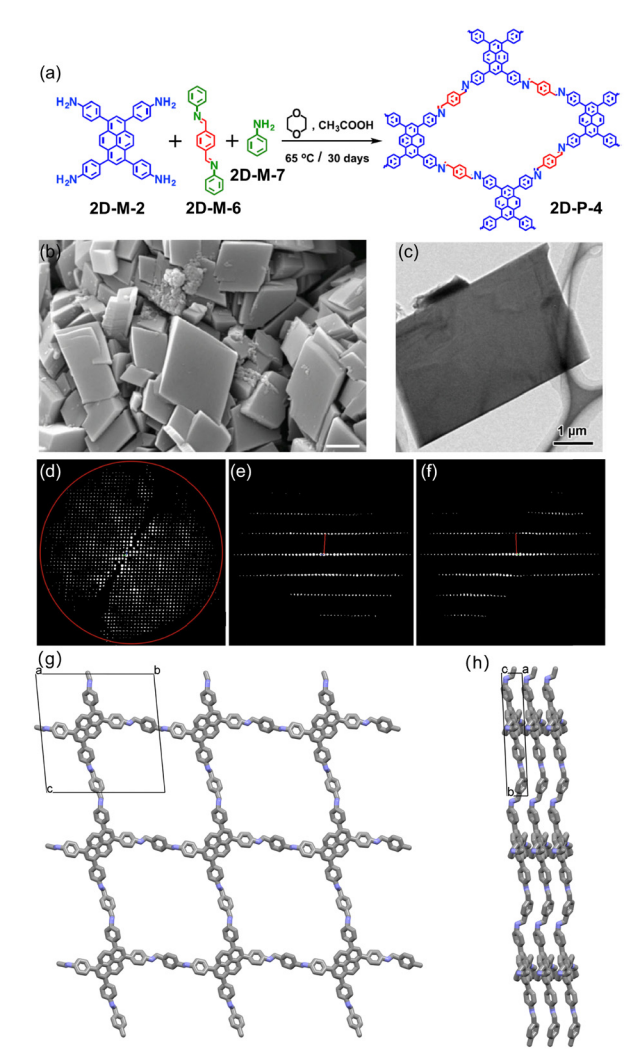


Fig. 16 Examples of solution phase synthesis of single crystal 2D COFs: (a) synthesis of 2D-P-4; (b) SEM image of 2D-P-4 crystals; (c) TEM image of 2D-P-4 crystals; (d)-(f) 3D reciprocal lattice of 2D-P-4 reconstructed from the cRED data viewing along the (d) [100], (e) [010], and (f) [001] directions. (g) Single crystal structure of **2D-P-4** (view from c-axis). (g) Single crystal structure of **2D-P-4** (view from the *b*-axis). Reproduced with permission from ref. 170, Copyright 2022, Springer Nature.

along the c-axis in the pyrene-based 2D COFs. In fact, the synchronized offset stacking in 2D COFs has been well investigated previously by Bein and co-workers. 171,172 The consecutive COF sheets can be locked in position during crystal growth, thus minimizing the occurrence of stacking faults and dislocations. The propeller-shaped molecular building units, such as tetraphenylethylene and triphenylamine, or pyrene units with substituents on the core, can generate well-defined periodic docking sites, which guide the assembly of successive layers. As a result, the long-range ordered stacking was promoted during the COF formation.

3.2 Topochemical polymerization

As discussed previously, confining the polymerization within a 2D plane and creating long-range order along the c-axis through stacking in solution could be challenging. In this context, SCSC

transformation provides a viable alternative, which involves the preorganization of monomers in a crystal lattice and their polymerization in the solid state. Similar to the 1D SCPs cases, this approach requires a proper packing of monomers with a specific orientation of reactive sites in each layer so that the polymerization can occur later between monomers within the 2D layer and form 2D SCPs. However, the control of crystal packing of monomers in the desired manner is challenging. It has been mainly based on chemical intuition and the continuous trial-and-error process, which frequently leads to undesired packing motifs. Additionally, during the SCSC transformation, cracking of the single crystal sometimes happens because of the lattice contractions or expansions during the polymerization process, which can also make SCXRD analysis not feasible. Although there have been many challenges in such a process, researchers have achieved several successful examples of 2D SCPs through topochemical polymerization.

In 2009, Schlüter raised an interesting question: "Twodimensional polymers: just a dream of synthetic chemists?"173 The synthesis of these polymeric materials, which are atom thin, covalently bonded, and in long-range order, represents a grand challenge. In 2014, Schlüter and co-workers reported the first successful synthesis of a 2D SCP through SCSC. 9 The rotorshaped anthracene-based monomer 2D-M-8 is composed of three anthracenes as blades (Fig. 17b). The packing behavior of the solvent for growing the crystal was investigated. After many attempts, cyanopyridine was finally found to be a suitable solvent in which a face-to-face arrangement of anthracene units was achieved in the single-crystal structure of 2D-M-8 (Fig. 17c). A model study was conducted using a simple anthracene derivative, which confirmed the feasibility of such an approach (Fig. 17a). A successful formation of the extended 2D network with an interlayer distance of around 3.6 Å was then followed.

In detail, the monomer single crystals with sizes $> 200 \mu m$ were irradiated for 48 hours with blue light (465 nm) to form 2D-P-5 via [4+4] photo-cycloaddition (Fig. 17d). The size of 2D-P-5 is dependent on the monomer single crystal grown from the solution. Both the exact structures of the monomer 2D-M-8 and the obtained 2D-P-5 were confirmed by regular SCXRD analysis.

During the same period, King and co-workers also independently designed a triptycene-based monomer (2D-M-9) which contains three anthracene moieties as blades (Fig. 17e).80 Every "blade" contains four fluorine atoms at the outer rim of the anthracene. By using the same [4+4] cycloaddition chemistry, a similar 2D SCP was obtained. The single crystal of the monomer 2D-M-9 was grown in chloroform, which has a 2D layered packing based on SCXRD. Each layer consists of 2D-M-9 monomers stacked facing each other in a quasi-hexagonal packing arrangement (Fig. 17f). The blue light (400-460 nm) triggered the [4+4] photo-dimerization, which led to the SCSC transformation to yield a 2D SCP 2D-P-6 (Fig. 17f). Notably, an intermediate dimer crystal was observed during the early stage of photopolymerization (460 nm) in the single crystal state. The 2D-P-6 single crystal was obtained after elongated ultraviolet irradiation (400 nm) of the dimer crystal at 223 K (Fig. 17f). These pioneering works in the preparation of 2D SCPs have received significant scientific attention, 9,80 and opened new possibilities for making 2D SCPs by controlling the growth of single crystals of well-designed monomers rather than controlling the polymerization conditions (conventional approach).

Besides [4+4] photo-dimerization of anthracenes in the solid state for making 2D SCPs, [2+2] cycloaddition was also successfully applied in the SCSC process. Schlüter and co-workers designed a pyrylium-based triolefinic monomer 2D-M-10 (Fig. 18a).¹⁷⁴ A single crystal of 2D-M-10 was obtained in a

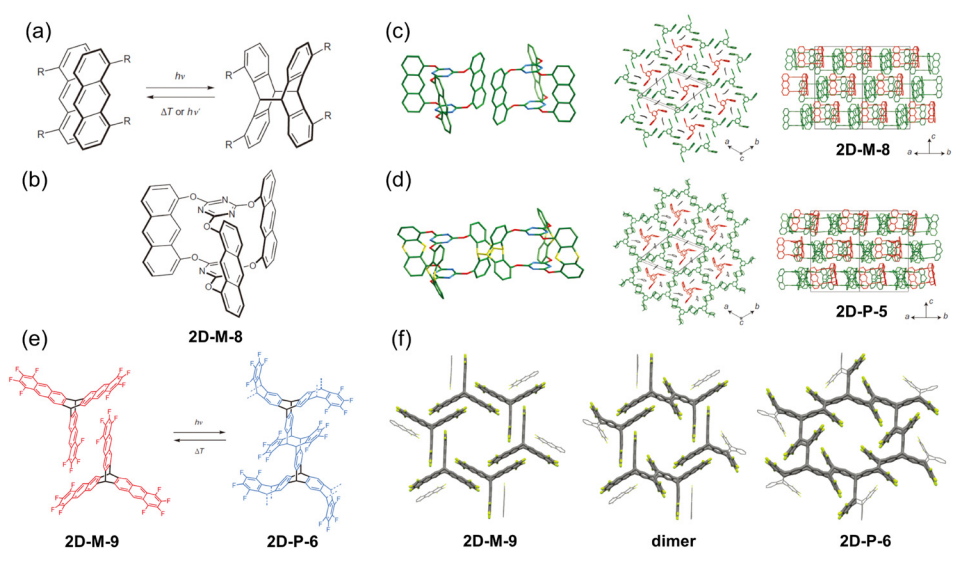


Fig. 17 The pioneering topochemical polymerization approaches to obtaining 2D SCPs: (a) a model reaction of the photochemical dimerization of anthracenes derivatives. (b) Molecular structure of 2D-M-8; (c) the crystal structure and the packing mode of 2D-M-8; (d) the crystal structure and the packing mode of 2D-P-5; (e) structures of 2D-M-9 and the corresponding 2D-P-6; (f) the crystal structures of the 2D-M-9 and the corresponding 2D-P-6. Reproduced with permission from ref. 80 and 173, Copyright 2014, Springer Nature.

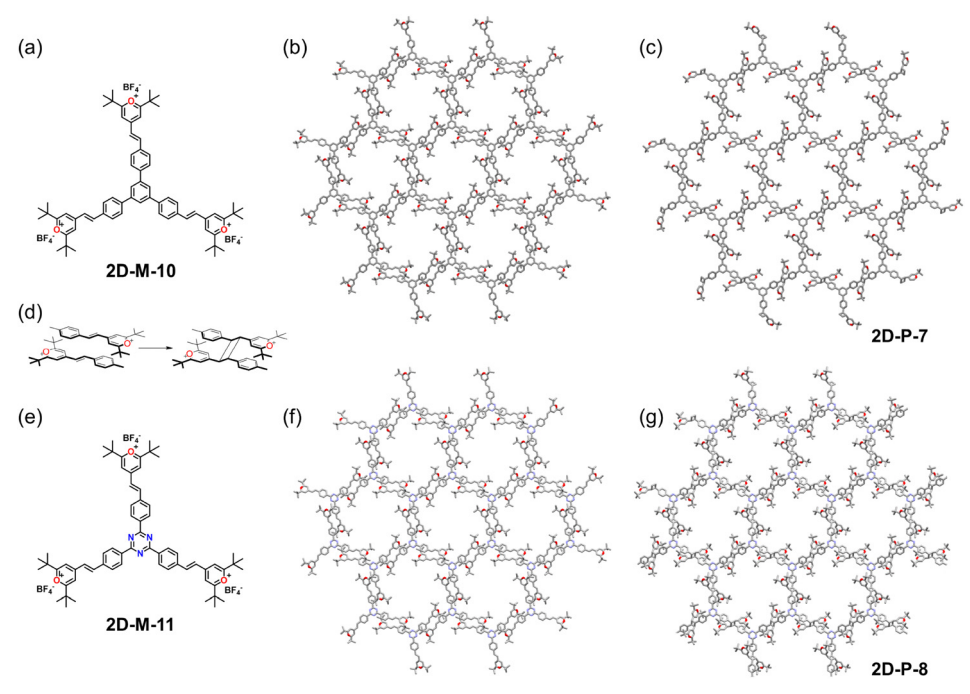


Fig. 18 Topochemical polymerization approach to obtain 2D SCPs through [2+2] cycloaddition: (a) structure of 2D-M-10; (b) single-crystal structure of one layer of 2D-M-10; (c) single-crystal structure of one layer of 2D-P-7; (d) dimerization of the model compound; (e) chemical structure of 2D-M-11; (f) single-crystal structure of one layer of 2D-M-11; (q) single-crystal structure of one layer of 2D-P-8.

mixture of acetic and formic acids. Monomer 2D-M-10 crystallized into a layered structure with a distance of 3.9 Å between the neighboring olefin moieties of 2D-M-10 (Fig. 18b), which meets the Schmidt criterion for the topochemical reaction. 175 Irradiation (530 nm) at 4 °C induced a color change of the crystals from orange to yellow, indicating the interrupted conjugation and the occurrence of polymerization. A novel 2D polymer (2D-P-7) with pyrylium units was formed upon the completion of the polymerization. As shown in Fig. 18c, six pyrylium units point inside each pore of 2D-P-7, fully decorating the pores with positively charged pyrylium groups. This feature may provide a novel 2D polymer with excellent polyelectrolyte properties.

Zhao and co-workers reported another example of a 2D SCP through SCSC transformation using monomer 2D-M-11, which is similar to monomer 2D-M-10 (Fig. 18e). 176 Triazine was used as the core instead of the benzene ring. Fortunately, the structural alteration does not cause a significant change in the crystal packing of 2D-M-11 compared to monomer 2D-M-10. In 2D-M-11, three arms were packed head-to-tail to form a hexagon (Fig. 18f). Given the distance between neighboring styryl units (3.919 Å), the [2+2]-photo-cycloaddition could take place. Upon irradiation with 530 nm light for 12 hours, the crystal underwent a color change from dark yellow to light yellow, while still maintaining the translucent feature. SCXRD confirmed the successful polymerization and the formation of a 2D polymer (2D-P-8). The hexagonal honeycomb porous structures were formed in each layer with a pore diameter of 2.7 nm (Fig. 18g). Notably, it was found that a minor change in the monomer structure could play a critical role in the layer

exfoliation process. The addition of CF3COOH (TFA) led to the protonation of the triazine core and introduced repulsive forces between layers due to charge and/or steric effects, thus facilitating the exfoliation process. More than 60% of the monolayered 2D polymer was found in a clear solution-like sample in TFA/gamma-butyrolactone (GBL).

All the examples mentioned above involve the topochemical polymerization of a single type of rigid monomer. Simultaneous integration of the features with high flexibility and high crystallinity into porous polymers is particularly challenging. Ke and co-workers reported a series of single-crystal organic frameworks crosslinked by H-bonds, which are named hydrogenbonded cross-linked organic frameworks (H_COF). The flexibility and crystallinity are integrated into a single framework of H_COF (Fig. 19).¹⁷⁷ Similar to the topochemical polymerization, it is necessary to preorganize the monomers through H-bonding interactions. 160,178 Subsequently, a second component, such as alkyldithiols, was introduced as flexible crosslinkers. The single crystals were photo-polymerized via thiol-ene or thiol-yne reactions through SCSC transformation.

As shown in Fig. 19a and b, monomer 2D-M-12, containing a tetraphenylethylene core with four melamine units and eight allyl groups, was designed and synthesized. A single crystal of monomer 2D-M-12 was obtained through slow vapor diffusion of MeCN into DMF solutions. Subsequently, flexible alkyldithiols with different lengths (2D-M-13, 2D-M-14) were introduced into the monomer crystal as the crosslinkers through diffusion. UV irradiation yielded 3D-P-1 and 2D-P-9. SCXRD analysis showed that 2D-P-9, which was synthesized with a short crosslinker, formed a 2D network, whereas 3D-P-1, which

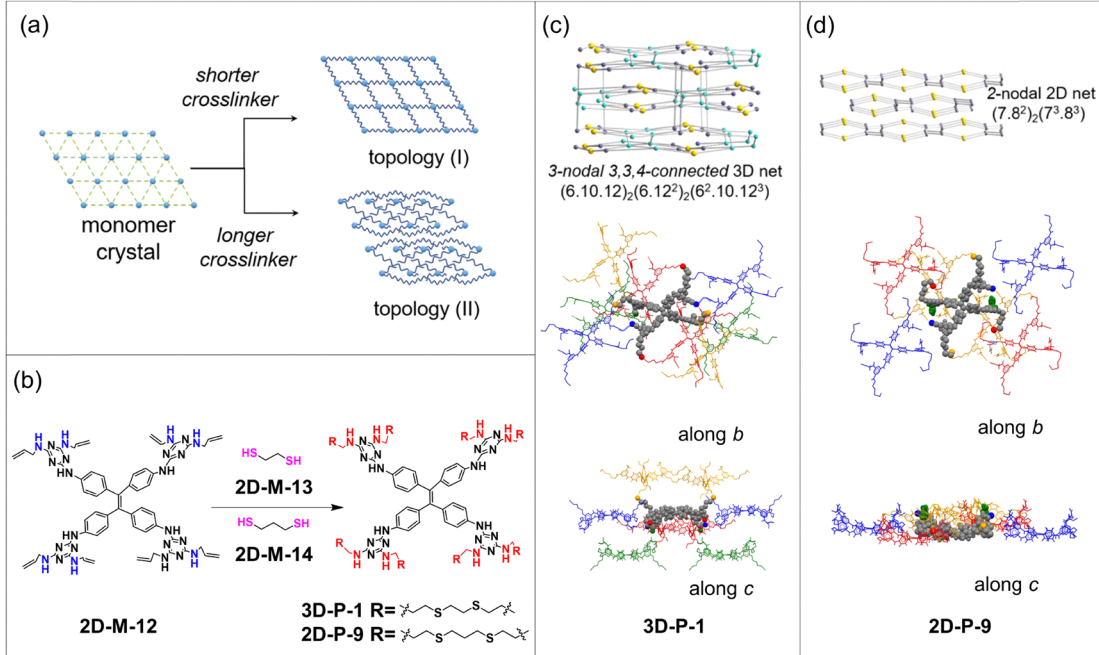


Fig. 19 Topochemical crosslinking of monomers with flexible linkers: (a) schematic representation of the synthesis of H_COFs materials; (b) synthesis of 3D-P-1 and 2D-P-9; (c) the topology and single-crystal structure of 3D-P-1; (d) the topology and single-crystal structure of 2D-P-9. Reproduced with permission from ref. 177, Copyright 2019, American Chemical Society.

was synthesized with a longer crosslinker, formed a 3D interconnected network (Fig. 19a). As shown in Fig. 19c and d, 2D-P-9 is a 2-nodal 3,4-connected 2D network in which two neighboring layers of the monomer 2D-M-12 are covalently crosslinked and extended along the [010] plane. In contrast, 3D-P-1 is an interconnected 3D network exhibiting a 3-nodal 3,3,4-connected selfentangled structure.

The same group subsequently reported another 2D SCP through a similar strategy.¹⁷⁹ As shown in Fig. 20a, a 2D hexagonal H-bonded structure was first formed via a co-crystallization of 2D-M-15 and 2D-M-16. 2D-P-10 was then obtained via an SCSC transformation through thiol-ene crosslinking (Fig. 20a). The heteromeric co-crystallization of two COOH-based monomers led to a suitable packing mode of the crystal, allowing the subsequent thiol-ene reaction. In 2D-P-10, the dithioether linkage A was found to connect 2D-M-15 in non-adjacent 1,4-layers, while the linkages C and D connect two allyl groups in 1,3-layers (Fig. 20b and c). The linkage B connects 1,2- and 1,3-layers, forming a 2D structure with flexible interlayer cross-linkages. This example showcases an interesting strategy for achieving the desired packing of monomers with the positioning and orientation necessary for interlayer crosslinking to form 2D polymers through co-crystallization using a complementary set of monomers.

Ke and co-workers recently reported 2D porous single crystals that are formed from a three-arm monomer (2D-M-17) consisting of piperazine and diallylmelamine moieties (Fig. 21a). 180 Due to piperazine's semi-rigid chair conformation, the π - π interactions between stacked layers in the solid state are reduced. The assembly of 2D-M-17 with an anion, HSO₄-, formed porous single crystals with unique tris-anion (HSO₄⁻)₃ clusters.

The subsequent thiol-ene SCSC transformation through photoirradiation covalently crosslinked the allyl groups in the preorganized molecular crystal, forming a 2D SCP (2D-P-11) with large voids (Fig. 21c). Notably, 2D-P-11 exhibited rapid and reversible size expansion and contraction (>200%) upon a guest uptake and switching between crystalline and amorphous phases due to the guest-induced disruption of the anion cluster.

These studies hold great promise for achieving both high crystallinity and flexibility in organic frameworks. Achieving the optimal balance between rigidity and flexibility while keeping the single crystal state before and after the reaction is the critical factor for the success of HcOF single crystals formation. So far, the reaction to form the H_COF has been limited to the topochemical thiol-ene cycloaddition, which requires the vinyl group in the parent molecules and thiol groups in the flexible crosslinkers. The concept of a rigid-flexible combined strategy has proven to be effective in the construction of 2D SCPs. By introducing second components as crosslinkers to covalently connect the parent molecules in an SCSC manner, the need for an extremely strict 2D packing mode for the monomers in the single-crystal state, as in the single-component topochemical polymerization, could be avoided. Guest-induced changes in the void structure of H_COF could have intriguing applications in selective adsorption and release of guests with high capacity.

3.3 Other approaches

As is well known, the key to 2D graphene preparation is obtaining the monolayered graphene, which is normally obtained through the exfoliation of the bulk graphite.3 The advantages of the 2D structure are most evident in the case of

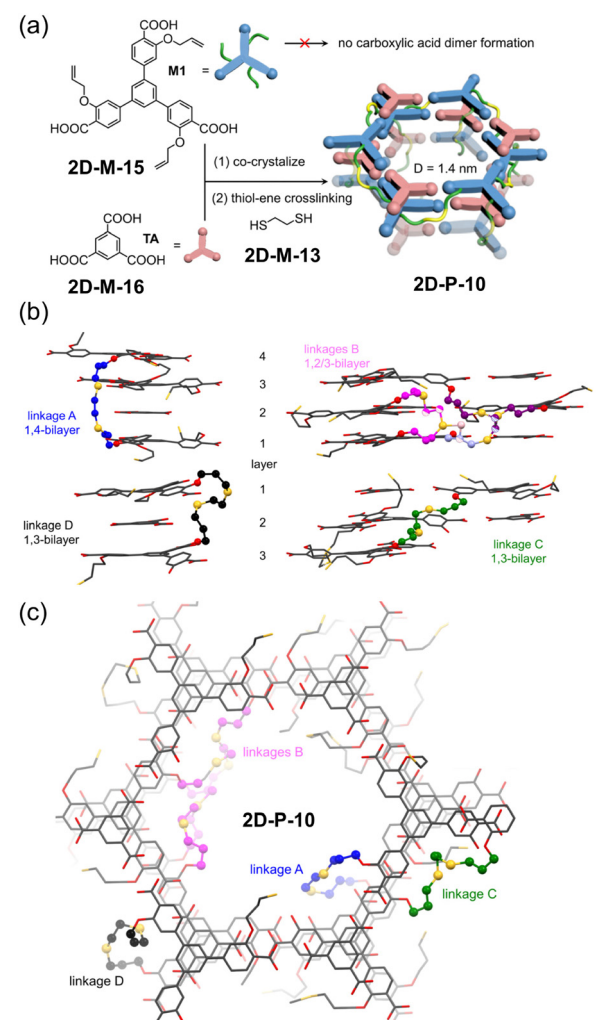


Fig. 20 Layered packing of monomers enabled by co-crystallization and subsequent topochemical crosslinking: (a) synthesis of 2D-P-10; (b) dissected sections of 2D-P-10; (c) single-crystal structure of 2D-P-10. Reproduced with permission from ref. 179, Copyright 2021, Wiley-VCH.

monolayered graphene. Similar to the production of monolayered graphene, the preparation of a monolayer 2D polymer undoubtedly represents a grand challenge in this field. 176,181 It is now possible to obtain large-sized 2D SCPs in a synthesis lab, but controlling the exfoliation process to achieve a monolayer with good dispersity through the so-called "top-down" strategy presents a significant challenge. 176,182-188 An alternative approach to preparing monolayered, large-sized, and free-standing 2D polymers is through "bottom-up" interfacial synthesis. This approach takes advantage of the template and confinement effect of an interface, allowing for pre-assembly of the monomers at an air/ water interface to yield a single-crystalline 2D polymer film. 189-193 Although there is no direct evidence from SCXRD, the structures of these ultra-thin 2D polymers have been assumed to be welldefined according to the characterization of the selected area electron diffraction (SAED), high-resolution transmission electron microscopy (HRTEM) or high-resolution atomic force microscopy (HRAFM). To date, many crystalline 2D polymer films have been successfully prepared through interfacial synthesis. 192,194-203

Several excellent reviews have summarized examples. 173,193,204,205 Thus, they are not covered in detail here.

Just as nature creates 2D graphite or 3D diamond, C60-based SCP has also been obtained under extreme conditions, such as high pressures in the range of several GPa in a laboratory setting. 206-209 High-pressure polymerization of C₆₀ has been widely studied through [2+2] cycloaddition. 210,211 Three polymeric phases, including 1D orthorhombic (O), 2D tetragonal (T), and 2D rhombohedral (3R) phases, have been reported for these polymers. Yamanaka and co-workers obtained the singledomain crystals of the 3R 2D C₆₀ polymer (2D-P-12) under high pressure of 5 GPa at 773 K.²⁰⁶ As shown in Fig. 22a, the crystal structure of 2D-P-12 consists of a hexagonal 2D layered structure formed by the polymerization of C₆₀ molecules through [2+2] cycloaddition. The unit cell adopts an ABC stacking mode along the c-axis, with the layers held together through van der Waals forces (Fig. 22b).

Since the discovery of the first fullerene C₆₀, the reactivity and different reactions of C₆₀ have been widely studied, ^{212,213} including the reaction of C₆₀ with alkaline earth metals. ²¹⁴⁻²¹⁶ Several single-crystal examples of metal-doped fullerene polymers prepared through vapor-phase growth at normal pressure have been reported. 213,217-219 For example, Tanaka et al. synthesized a single crystal of Mg-doped 2D fullerene polymers (2D-P-13) through a binary vapor-phase mixture of Mg and C₆₀ in sealed glass tubes at elevated temperatures (Fig. 23).²²⁰ The mixture was placed in a two-zone furnace with a temperature gradient of 500-600 °C for 24 hours, and the single crystals were obtained in the zone of lower temperature (500 °C). The crystal structure revealed that the C₆₀ molecules were connected along the a and b axis to form a 2D layer, which is stacked along the c-axis in an AB stacking mode, with Mg atoms intercalated between the layers at an Mg-C distance smaller than 2.7 Å.

Recently, Zheng and co-workers successfully exfoliated 2D magnesium-doped C₆₀ SCPs using a cation intercalation method.²²¹ Two different Mg-intercalated single crystals of 2D. C₆₀ polymers with quasi-hexagonal (2D-P-14) and quasi-tetragonal (2D-P-15) structures were obtained through a facile reaction at atmospheric pressure by adjusting the ratio of Mg and C₆₀ (Fig. 24a and b). The subsequent introduction of tetrabutylammonium salicylate (TBAS) cleaved the C-Mg bonds between C60 polymer layers and tetrabutylammonium (NBu4+) cations and replaced Mg ions in the interlayer. The larger ionic radius of NBu⁴⁺ led to an effective expansion of interlayers, facilitating exfoliation (Fig. 24c). Due to the asymmetric lattice structure derived from the orderly arrangement of asymmetric C₆₀ cages, the single layer of 2D-P-15 exhibited in-plane anisotropic behavior, including anisotropic phonon modes and conductivity. With a bandgap of 1.6 eV, the single-layered 2D C₆₀ polymer has great potential for applications in optoelectronics.

4 3D architectures

Diamond represents an excellent example of 3D SCPs. Synthetic strategies for 3D SCPs are similar to those used for 2D SCPs,

Review Article

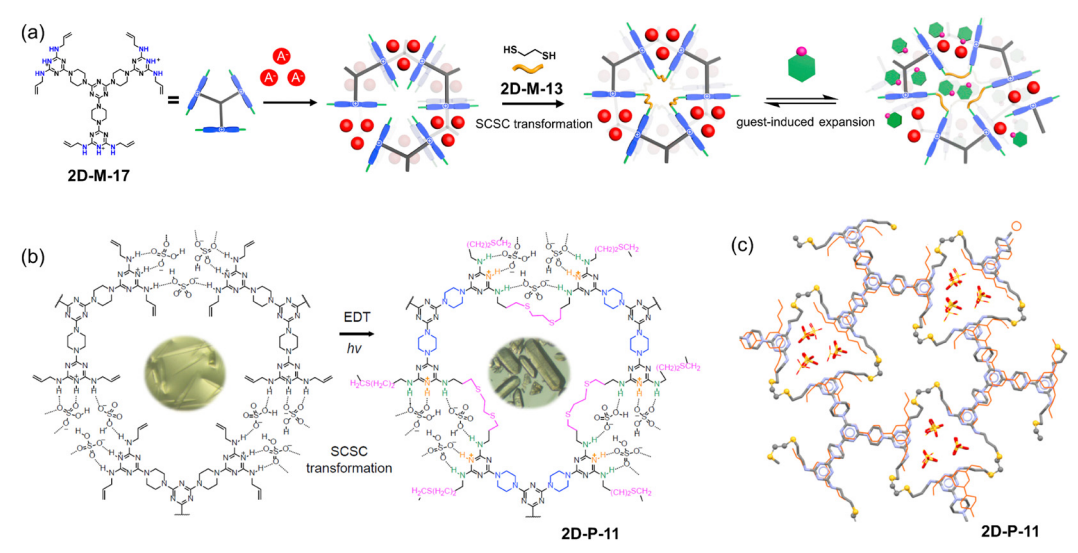


Fig. 21 Crystallization of monomers through ion-cluster formation and their topochemical crosslinking: (a) illustration of the anion-cluster-directed formation of a hexagonal hydrogen-bonded network, conversion to 2D-P-11 through SCSC crosslinking, and the guest uptake process. (b) Synthesis of 2D-P-11 through thiol-ene SCSC transformation. (c) Single crystal structure of 2D-P-11. Reproduced with permission from ref. 180, Copyright 2022, Elsevier.

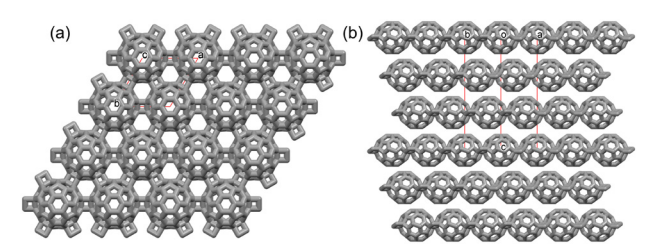


Fig. 22 2D fullerene SCP: (a) single-crystal structure of monolayer of 2D-P-12; (b) ABC packing mode of 2D-P-12 in a single crystal.

which include solution synthesis, topochemical synthesis, and high-pressure synthesis. It is worth noting that there are more successful examples of solution-synthesized 3D SCPs than 2D SCPs. Conversely, there are more examples of topochemically synthesized 2D SCPs than 3D SCPs. Likely, the growth in 3D orientations may favor the formation of 3D structures in solution, whereas the possible slippage between the layers in 2D SCPs hinders the growth of single crystals. Thus, for 2D SCPs, topochemical synthesis has been more successful than solution synthesis.

4.1 Solution synthesis

4.1.1 Modulator-assisted synthesis. Wang, Yaghi, and Sun developed a general strategy for the synthesis of large-sized single crystals of 3D COFs.11 The key step of achieving good crystallinity is the efficient self-correction of defects. The authors envisioned improving the reversibility of the imine bond which could facilitate the formation of high-quality crystals. This was accomplished by introducing an excess of aniline, which could act as a competitive modulator and a nucleation inhibitor. The excess aniline could slow down the reaction rates and facilitate the self-correction process. As a

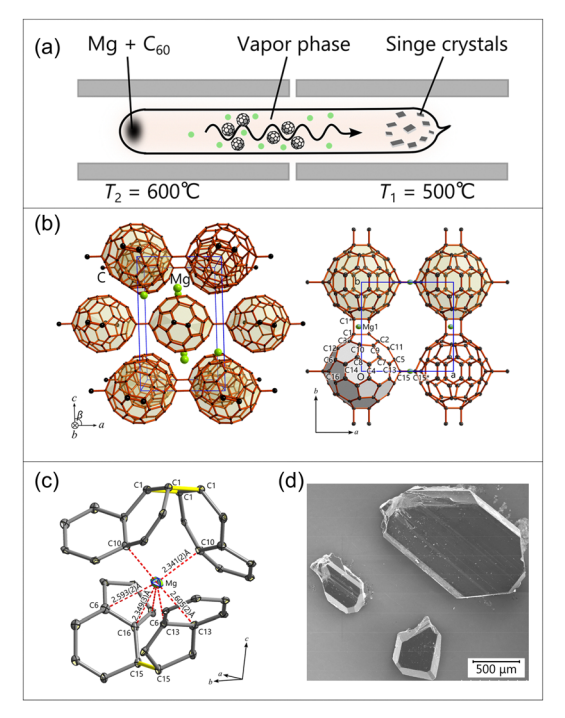


Fig. 23 Mg-doped 2D fullerene SCP: (a) schematic picture of the equipment for the synthesis of Mg-doped fullerene polymer 2D-P-13. (b) Singlecrystal structure of 2D-P-13. (c) Carbon coordination surrounding the Mg atom. (d) SEM image of 2D-P-13 single crystal. Reproduced with permission from ref. 220, Copyright 2018, American Chemical Society.

result, large-sized single crystals were obtained. Four 3D COF single crystals with uniform blocks (3D-P-2, 3D-P-3, 3D-P-4, and **3D-P-5**) were obtained by using this modulation strategy (Fig. 25). The large size and high quality of the single crystals enabled unambiguous structure elucidation through SCXRD analysis. The

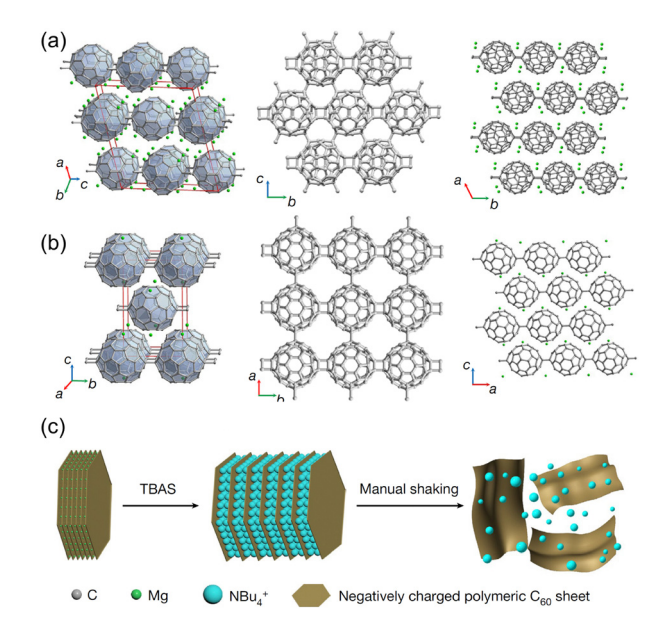


Fig. 24 Exfoliation of 2D fullerene SCP: (a) single-crystal structure of 2D-P-14. (b) Single-crystal structure of 2D-P-15. (c) Schematic of the exfoliation process. Reproduced with permission from ref. 221, Copyright 2022, Springer Nature

commonly encountered ambiguities of interpenetration in 3D COFs, the location of the guest molecules, the imine bond formation, and the determination of complicated topology were clearly deciphered with atomic resolution, which could not be accomplished by using common PXRD characterization.

Applying this modulation strategy, Wang and co-workers further reported a non-interpenetrated COF (3D-P-6).222 Quadrilateral and tetrahedral linkers consisting of tetraphenylethylene and adamantane, respectively, were used as building blocks to construct a single-crystal 3D COF with a new topology and less interpenetration (Fig. 26a). By using the modulation strategy (adding a nucleation inhibitor and competitive modulator), single crystals of 3D-P-6 were obtained. SCXRD measurement on a single crystal with a size of 50 µm (Fig. 26d and e) using synchrotron light sources showed the tetragonal unit cell. Further cRED characterization confirmed the unit cell parameters. Based on the SCXRD and diffraction data, a non-interpenetrated open framework with a pts topology was established (Fig. 26b and c).

Wang, Sun, and co-workers designed a new tetrahedral node for constructing 3D COFs by introducing steric hindrance in the ortho positions of biphenyl cores to generate nonplanarity of the monomer (3D-M-9). The dihedral angles resulted in the formation of the tetrahedral building unit 3D-M-9 (Fig. 27).²²³ The size of 3D-P-7 crystals obtained through conventional solvothermal synthesis was very small. However, when aniline was added as a modulator under optimized conditions, 3D-P-7 with a larger crystal size was successfully obtained, which could be analyzed by cRED with a resolution of 2 Å. The structure analysis showed that 3D-P-7 adopts a 7-fold interpenetrated structure with pts topology. Although the number of successful examples is still minuscule, the modulation strategy has shown great potential in synthesizing single-crystal 3D COFs with tunable sizes, especially the preparation of large-sized singlecrystal 3D COFs for SCXRD analysis.

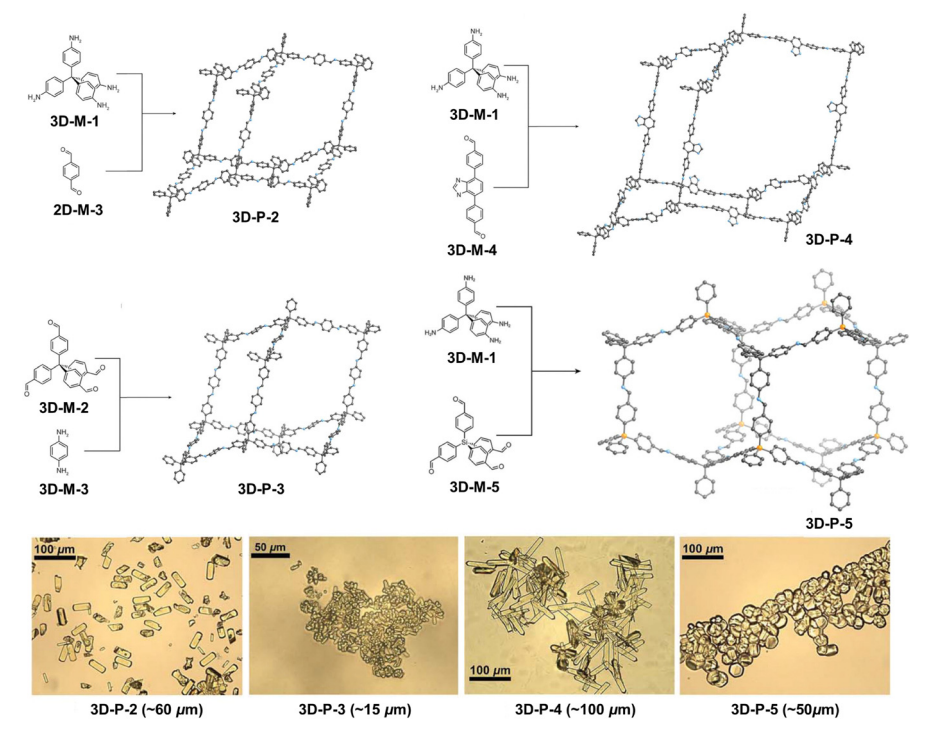


Fig. 25 The synthesis and single-crystal structures of four 3D COFs (3D-P-2, 3D-P-3, 3D-P-4, and 3D-P-5) and the corresponding optical microscopy images. Reproduced with permission from ref. 11, Copyright 2018, American Association for the Advancement of Science.

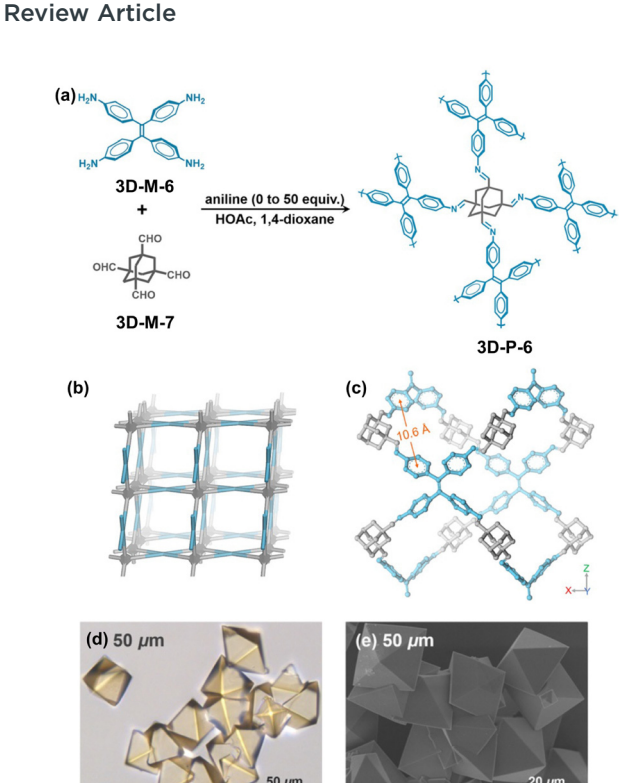


Fig. 26 Non-interpenetrated 3D COF: (a) synthesis of single-crystal COFs 3D-P-6. (b) Non-interpenetrated pts topology. (c) Crystal structure of 3D-P-6. (d) The optical microscopy image of 3D-P-6. (e) SEM image of single-crystal 3D-P-6. Reproduced with permission from ref. 222, Copyright 2020, Wiley-VCH.

4.1.2 Conventional solvothermal synthesis. As mentioned previously, conventional solvothermal synthesis typically yields polycrystalline powders instead of high-quality single crystals. Nevertheless, under optimized reaction conditions, the synthesis can yield single-crystal 3D COFs, although the sizes are usually too small to be analyzed by SCXRD. cRED has emerged as a powerful alternative method for characterizing small single

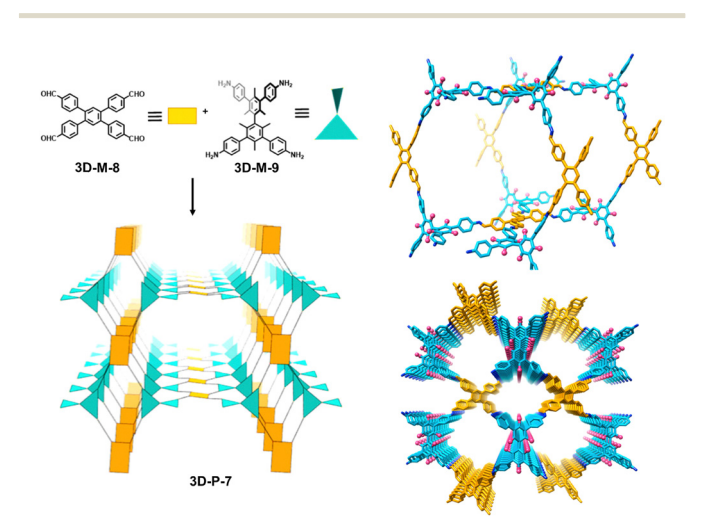


Fig. 27 Synthesis and the single-crystal structure of 3D-P-7. Reproduced with permission from ref. 223, Copyright 2020, American Chemical Society.

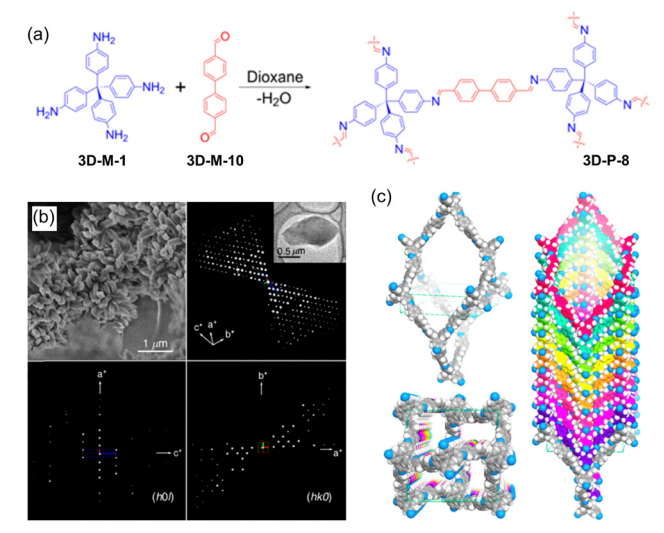


Fig. 28 The cRED technique for the structure determination of 3D COF: (a) synthesis of 3D-P-8. (b) Morphology and electron diffraction of 3D-P-8. (c) Single-crystal structure of **3D-P-8**. Reproduced with permission from ref. 16, Copyright 2013, American Chemical Society.

crystal structures. 15,16 In 2013, Yaghi and co-workers reported a cRED technique for the structure determination of a 3D COF (3D-P-8) (Fig. 28). 16 After collecting the cRED data, the 3D reciprocal lattice was reconstructed with a resolution of up to 1.5 Å (Fig. 28b) and the structure of 3D-P-8 was successfully determined in the space group $I\bar{4}2d$ (Fig. 28c).

Wang and Sun further explored such a method and employed a 3D cRED technique to determine the structures. 14,223,224 They developed a novel topology design approach for constructing 3D COFs from tetrahedral or quadrilateral building blocks. Iminelinked 3D COF isostructures (3D-P-9, 3D-P-10, and 3D-P-11) were synthesized through a "4+4" reaction (Fig. 29a). 14 After optimization of the reaction condition, single crystals with an octahedral shape and size up to 1 µm were obtained (Fig. 29c). The 3D cRED technique proved capable of resolving the locations of the atoms except for H in the 3D structures of 3D-P-9, 3D-P-10, and 3D-P-11, which show 5-fold interpenetrated pts nets with a resolution of 0.9 Å (Fig. 29b).

The development of the cRED technique allows us to explore the changes in topology through steric control. As shown in Fig. 30a and b, Wang and Sun synthesized three 3D COFs from similar precursors. The change in the substituents from methoxy groups to phenyl groups in the monomers changed the topology of the corresponding 3D COFs accordingly. 225 Two 3D COFs with totally different topologies were obtained. Based on cRED analysis, 3D-P-12 adopts a pts topology with a 5-fold interpenetrated structure, whereas 3D-P-13 was found to have a new ljh topology. When the substituents were changed to OH groups (3D-P-14), a reversible transformation was found in the switchable 3D COF through a quinone/hydroquinone redox reaction (Fig. 30c).²²⁶

As is widely recognized, rigid building blocks are typically used in synthesizing 3D COFs due to their preorganized structure, which can minimize system entropy loss and facilitate the

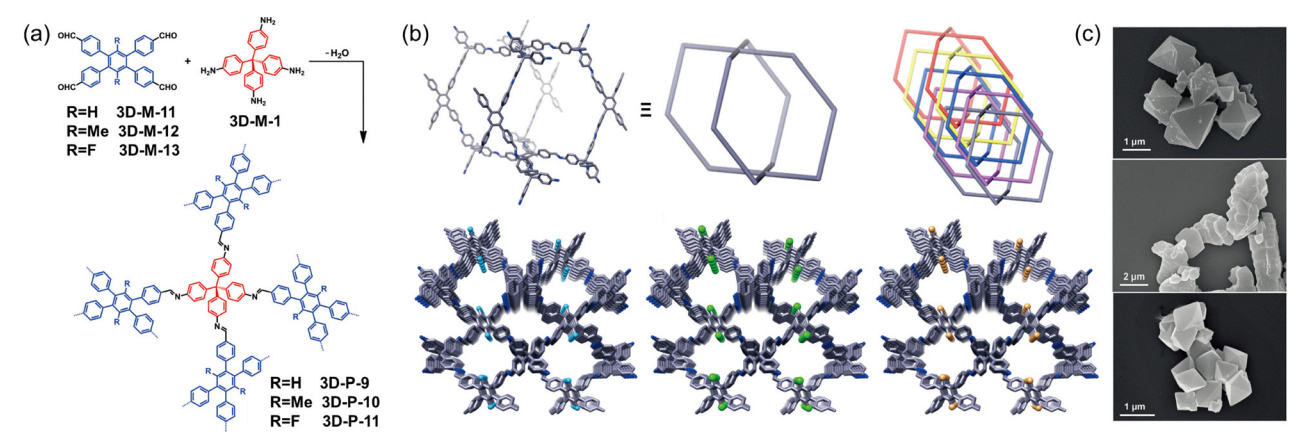


Fig. 29 The cRED technique for the structural determination of 3D COFs: (a) synthesis of three 3D COFs (3D-P-9, 3D-P-10, and 3D-P-11). (b) Structural representations of 3D-P-9, 3D-P-10, and 3D-P-11. (c) SEM images of 3D-P-9 (top), 3D-P-10 (middle), and 3D-P-11 (down). Reproduced with permission from ref. 14, Copyright 2019, Wiley-VCH

formation of ordered structures. Although the concept of constructing 3D COFs with flexible linkers is appealing, there have been only few successful examples reported due to the

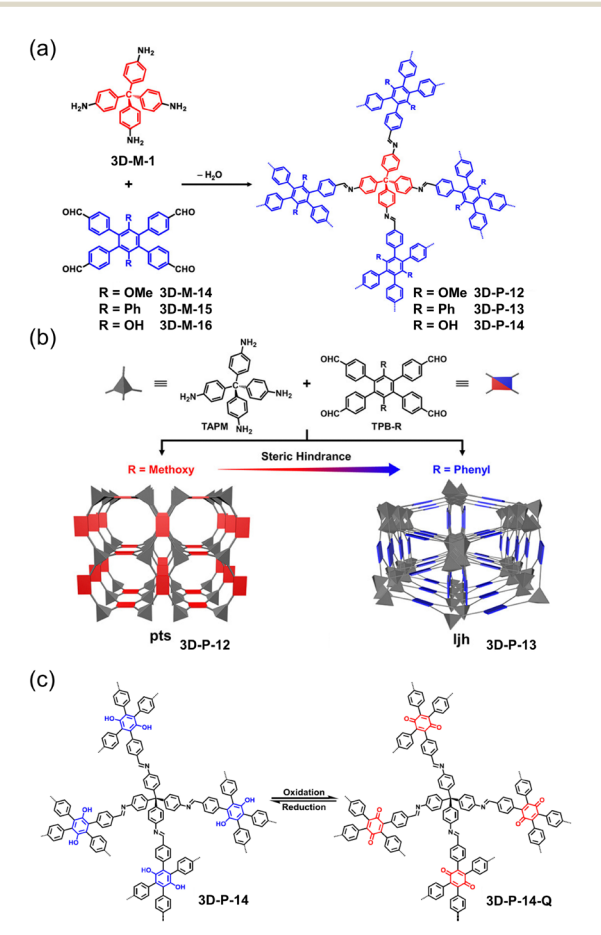


Fig. 30 Substituent effect on the topologies of 3D COFs: (a) synthesis of 3D-P-12, 3D-P-13, and 3D-P-14; reproduced with permission from ref. 225, Copyright 2021, American Chemical Society, (b) Tuning the topology of 3D-P-12 (pts) and 3D-P-13 (ljh) via steric control. (c) The oxidation and reduction process of 3D-P-14. Reproduced with permission from ref. 226, Copyright 2020, Springer Nature.

challenges in the synthesis and structure characterization. Flexible framework structures have demonstrated intriguing characteristics such as reversible expansion/contraction upon vapor adsorption/desorption and distinctive breathing behavior, establishing them as a new type of soft porous crystals. Recently, Wang and Sun reported a 3D COF (3D-P-15) with flexible ether linkages in the backbone (Fig. 31a). 224 Despite achieving a resolution of approximately 1 Å, direct determination of the structure of 3D-P-15 using cRED data was not possible due to the signal-to-noise ratio below 2 at high resolution (> 1.5 Å) and a completeness of around 40%. They, therefore, implemented an advanced data procession method typically used in protein structure determination, involving the scaling and merging of 17 cRED data sets. This ultimately led to the successful establishment of a complete structure model of 3D-P-15, adopting a pts topology with a 6-fold interpenetration (Fig. 31b). The flexibility of 3D-P-15 enabled by the flexible ether linkage allowed for a reversible expansion/contraction process upon vapor adsorption and desorption. However, the successful preparation of single crystal **3D-P-15** presented a significant challenge due to the free rotation of the C-O single bonds in the building block 3D-M-17. Achieving success required a judicious combination of the flexible 3D-M-17 and the rigid 3D-M-1 building block and numerous trials to identify optimized reaction conditions contributed to the success.

Conventional solvothermal synthesis has yielded many successful examples of small-sized, single-crystalline 3D COFs. $^{227,228}\,$ Unlike the case for 2D COFs, the growth in 3D directions in solution appears to favor the formation of ordered structures, while interlayer slippage, common in 2D COFs, is detrimental to crystallization. Nonetheless, optimizing reaction conditions for the preparation of single-crystal 3D COFs typically requires costly and time-consuming trial-and-error experiments, with no proven effective guidelines yet identified. With the technological development of characterization, particularly the cRED technique and the emergence of commercial instruments, it is expected that more and more diverse single-crystal 3D COFs will emerge. Moreover, the development of new types of organic reactions beyond the Schiff-base reaction would be of great interest, given

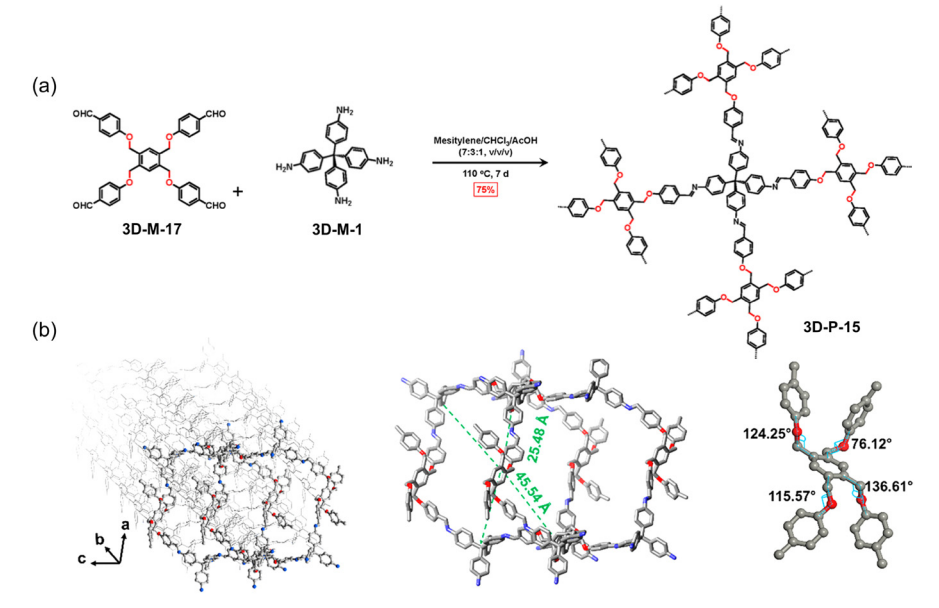


Fig. 31 An example of flexible 3D COF: (a) synthesis of 3D-P-15. (b) The single-crystal structure and the interpenetration of 3D-P-15. Reproduced with permission from ref. 224, Copyright 2021, American Chemical Society.

that current examples are all based on the formation of imine bonds.

4.1.3 Amphiphilic amino-acid assisted aqueous-phase synthesis. Recently, Zheng, Sun, Liu, and co-workers reported an amphiphilic-amino-acid-assisted strategy to prepare singlecrystal imine-linked COFs in aqueous solutions under ambient conditions.²²⁹ The amphiphilic amino-acid molecules can self-assemble into micelles and serve as dynamic barriers to prevent the precipitation of materials from the polymerization

of monomers in water, thus synthesizing single-crystal COFs (Fig. 32). This strategy shows good universality, and five types of 3D single-crystal COFs were obtained. 3D-M-1 is selected as the amine monomer, and 3D-M-18, 2D-M-3, 3D-M-10,3D-M-19, and 3D-M-20 containing electron-accepting, electron-donating, and heterocyclic groups next to the aldehydes are chosen as the aldehyde-based monomers. Palmitoylglycine (C₁₆-GlyA) acts as the amphiphilic amino-acid and can assemble into micelles with a layered supramolecular structure in water, affording a

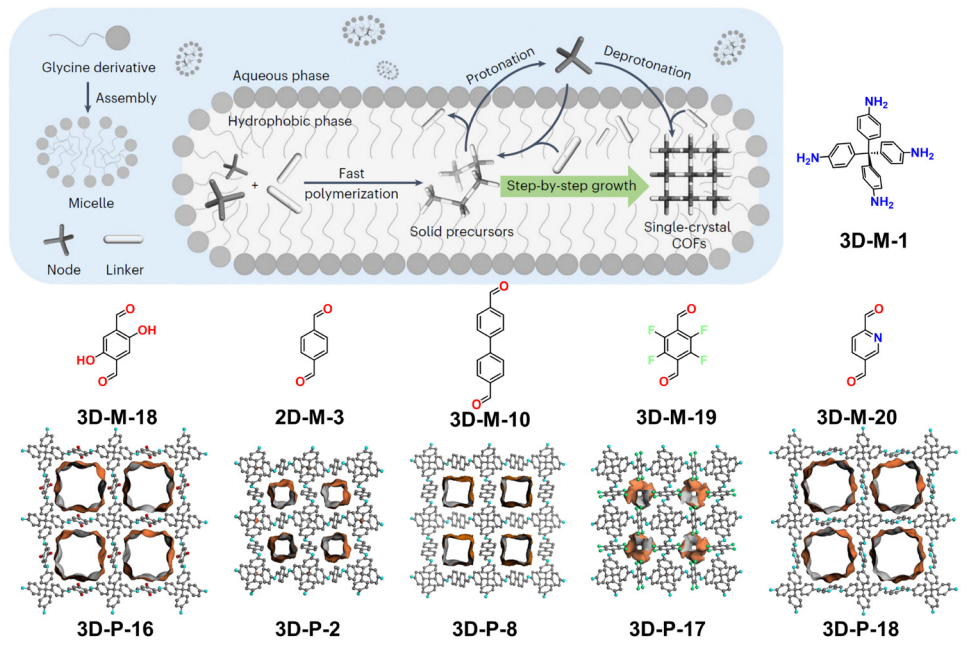


Fig. 32 Schematic diagram of the amphiphilic amino-acid-assisted aqueous-phase synthesis; chemical structures of monomer and single crystal structures of the prepared 3D COFs. Reproduced with permission from ref. 229, Copyright 2023, Springer Nature.

hydrophobic compartment. The aldehyde-based monomer was first dissolved into the C16-GlyA emulsion. The subsequent addition of p-toluenesulfonic acid-protonated 3D-M-1 led to gel-like mixtures, which are oligomers of polyimines. As the reaction proceeded, the disordered phase gradually transformed into crystals. Pure single-crystal COFs were obtained after a long-time reaction (14 days). The single-crystal structure of 3D-P-16 exhibits a diamond-type topology with seven-fold

interpenetration. 1D straight channels along the interpenetra-

tion direction were observed. The removal of C₁₆-GlyA leads to a

notable framework distortion. Similar to the case of 3D-P-16, all

non-hydrogen atoms of the 3D-P-2, 3D-P-8, 3D-P-17, and 3D-P-

18 crystals were identified. Notably, the single-crystal sizes of

3D-P-16 and 3D-P-18 are large enough for SCXRD analysis. The

Chem Soc Rev

three left structures were resolved by the cRED technique. 4.1.4 Metal-coordinated synthesis. Besides the traditional 3D COFs, Yaghi and co-workers developed a single-crystal 3D woven structure made of helical threads. The term "weaving" was used to describe the interlacing of 1D units that make 2D and 3D structures.²³⁰ Although these woven structures are made of 1D chains, the overall structures are 2D or 3D due to the metalcoordinated interaction to weave the 1D chains together.²³⁰ A starting material with tetrahedral geometry, the phenanthroline-Cu complex containing four aldehyde groups (Fig. 33a), was

chosen for the synthesis of a 3D COF via a Schiff base reaction

with the linear linker benzidine. The resulting imine-linked threads were precisely brought together by copper ions, which act as templates, yielding a 3D framework with a weaving arrangement. Thanks to the tetrahedral geometry of the phenanthroline-Cu complex, the threads can be assembled into the framework. The structure was resolved using 3D electron diffraction tomography (3D-EDT), which showed that 3D-P-19 has an orthorhombic Brayais lattice with a C-center, According to the refined model, 3D-P-19 crystallizes in a two-fold interpenetrated 3D framework with a dia topology. Notably, this material exhibits an unusual behavior in elasticity, likely because of its unique weaving structure. Subsequently, the same group used similar tetrahedral building units based on metal complexes to achieve a symmetrical arrangement of the organic threads to obtain a 3D woven structure with diamond topology (Fig. 33b).²³¹ The complex of cobalt and bis(diiminopyridine) acts as the tetrahedral building blocks with a dihedral angle of 80°. Unlike the previous study, the Boc-protected amine was used as the starting material, which was gradually deprotected to slow down the imine condensation reaction and facilitate the crystallization process. The structure of 3D-P-20 was solved by electron crystallography and X-ray analysis, showing 3D-P-20 has a very simple 3D woven structure. Only two sets of straight and parallel threads were observed in the structure to form one point of the registry.

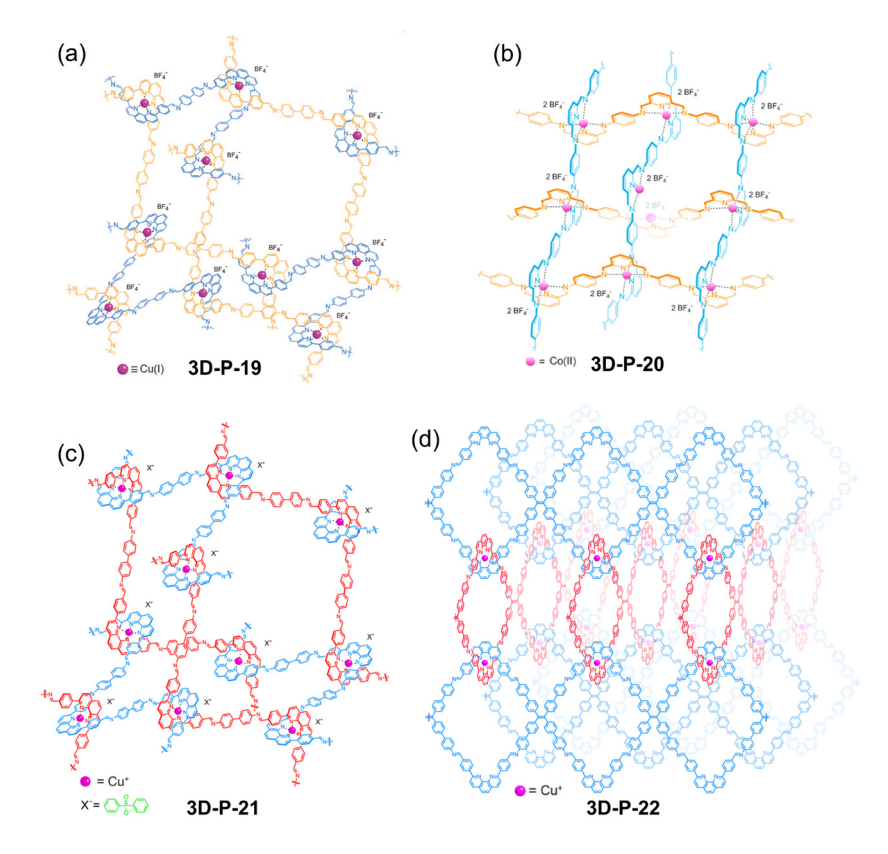


Fig. 33 Chemical structures of four examples of 3D woven COFs: (a) 3D-P-19. Reproduced with permission from ref. 230, Copyright 2016, American Association for the Advancement of Science. (b) 3D-P-20. Reproduced with permission from ref. 231, Copyright 2017, American Chemical Society. (c) 3D-P-21. Reproduced with permission from ref. 232, Copyright 2018, American Chemical Society. (d) 3D-P-22. Reproduced with permission from ref. 233, Copyright 2019, American Chemical Society

Based on the previous work of 3D-P-20, Yaghi and coworkers further reported a new isoreticular woven metallated **3D-P-21** (Fig. 33c). 232 In this work, the BF₄ counter anions were exchanged with PO₂Ph₂⁻ anions to fill the internal voids of the COFs. Thus, the interpenetration during the framework formation was successfully prevented in the case of 3D-P-21. 3D-EDT revealed a monoclinic Bravais lattice of 3D-P-21. The experimental PXRD pattern and HRTEM showed that 3D-P-21 belongs to the monoclinic space group Pc. Notably, 3D-P-21, which contains a 3D pore system with a large channel, exhibits adaptive dynamics for vapor and dye inclusion.

In a recent study, Yaghi and co-workers developed a new extended 3D COF structure with mechanical entanglement. 233 The framework was created by interlocking 1D ribbons of corner-sharing squares constituted entirely of covalently linked organic molecules (Fig. 33d). Similar to their previous work, they used the copper(1)-bisphenanthroline complex salt as the tetrahedral tetratopic units. However, instead of a linear ditopic benzidine linker, the square-planar tetratopic units were used to construct an extended 3D COF (3D-P-22) through interlocking of 1D corner-sharing square ribbons. The structure of 3D-P-22 with pts topology was revealed by electron microscopy and X-ray powder diffraction.

Loh and co-workers reported a 3D woven COF (3D-P-23), which was synthesized via the reaction between two stable metal complexes 1D-M-5 and 3D-M-21 (Fig. 34). 63 The structure of the 3D woven COF was characterized by 3D ED and PXRD. 3D-P-23 exhibits a dia topology with a three-fold interpenetrated structure. Cu ions in the tetrahedral building units serve as a node to organize the interlacing of the threads.

Crystalline woven materials are a valuable addition to the field of reticular chemistry, enriching the library of materials. It is possible to grow single crystals of these woven COFs. The presence of the metal may facilitate their crystallization. The structures of 3D woven COFs could be elucidated through a

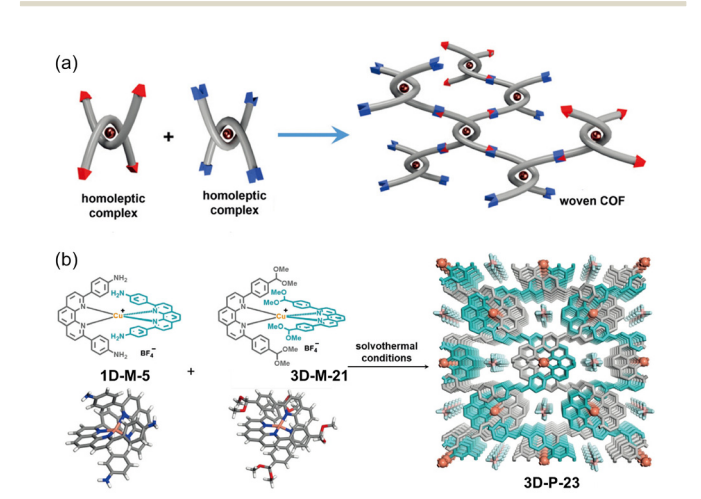


Fig. 34 3D woven COF: (a) the strategy of constructing 3D woven COF (3D-P-23); (b) the synthesis and the crystal structure of 3D-P-23. Reproduced with permission from ref. 63, Copyright 2023, Springer Nature.

combination of techniques, including the electron diffraction technique, PXRD, and HRTEM.

4.1.5 Exploration of new linkages. The majority of singlecrystal 3D COFs that have been reported in the literature are based on Schiff base chemistry and are synthesized by polycondensation of aldehydes and amines. The dynamic selfadjusting process is critical for achieving the thermodynamic equilibrium and ultimately forming highly ordered structures. However, exploring new reaction pathways for preparing singlecrystal 3D COFs with new linkages beyond the imine bond is highly encouraged and attractive. Despite numerous attempts to synthesize 3D COFs using novel linkages, successful examples of non-imine-bonded single-crystal 3D COFs with an unambiguous structure elucidation are very rare. In 2013, Wuest and co-workers reported several examples of single crystals of 3D covalent organic networks (3D-P-24, 3D-P-25, 3D-P-26). 10 The reversible self-addition polymerization of nitroso was utilized to realize the error-correction process. The authors found that the azodioxy linkers are suitable for the construction of singlecrystal covalent organic networks due to their good reversibility, which is the key to this strategy. Three different monomers with nitrous groups all converted to the corresponding diamondoid azodioxy networks as single crystals, which were characterized by SCXRD (Fig. 35a-c).

4.2 Topochemical polymerization

Unlike the topochemical approach used for the preparation of 2D SCPs, successful examples of 3D SCP preparation are extremely rare. Ke and co-workers reported one successful

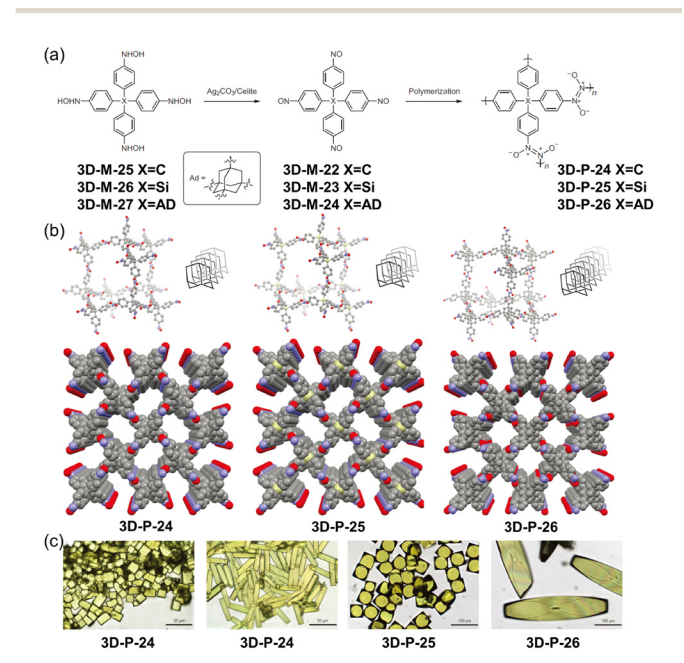


Fig. 35 Diamondoid azodioxy 3D SCPs: (a) synthesis of three covalent organic networks 3D-P-24, 3D-P-25, and 3D-P-26 by reversible selfaddition polymerizations. (b) Single-crystal structures of 3D-P-24, 3D-P-25, and 3D-P-26. (c) Optical microscopy images of the single crystals 3D-P-24, 3D-P-25, and 3D-P-26. Reproduced with permission from ref. 10, Copyright 2013, Springer Nature.

example (3D-P-1), which was discussed in Section 2.2 (Fig. 19) together with the 2D-P-9 with a 2D structure for the sake of organizational coherence. The design concept and synthetic strategy for 3D SCPs are similar to those of the 2D SCPs discussed in Section 2.2. While there are certainly challenges to overcome, as is also the case with the preparation of 2D SCPs, the current scarcity of successful examples is both intriguing and motivating for researchers to continue exploring this field. For example, Dincă and co-workers recently reported the preparation of crystalline 3D porous organic polymer with C-C bond linkages by using topochemical polymerization. Photoactive anthracene derivatives were connected to a tetraphenylmethane core to form the single-crystal monomer.²³⁴ Although the transformation from monomer to polymer through [4+4] photo-dimerization between the anthracene preserved crystallinity, efforts to obtain single crystals of the polymer were unsuccessful due to the large displacement of monomer molecules during the photopolymerization. While efforts to obtain single crystals of 3D polymers through [4+4] photo-dimerization have been unsuccessful. It is important to note that significant progress has been achieved, and the researchers were on the brink of success. Furthermore, the achievements in the field of 2D SCPs preparation through topochemical polymerization provide a solid foundation for the belief that rational monomer design and continued exploration will lead to the realization of 3D SCPs with promising properties.

4.3 Others

In addition to the traditional synthetic strategies, high-pressure synthesis offers an alternative method for preparing singlecrystal samples of 3D architectures, 208 as demonstrated by Yamanaka and co-workers in their work on 2D C_{60} SCP (discussed in Section 2.3).206,209 In 2006, they were able to convert the 2D C₆₀ SCPs into 3D C₆₀ SCPs (Fig. 36) using high pressure and temperature (15 GPa and 600 °C).²⁰⁸ The conversion occurred topochemically, preserving the basic structure of the individual 2D structure. The resulting single-crystal structure of 3D-P-27 revealed that each C₆₀ unit was deformed into a cuboid-shaped rectangular parallelepiped and linked to 8 cuboid neighbors in the body-centered cell by [3+3]

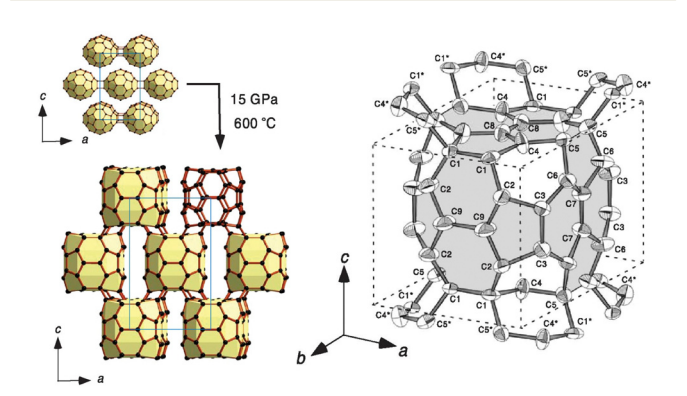


Fig. 36 Single-crystal structure of the 3D C60 SPC 3D-P-27. Reproduced with permission from ref. 208, Copyright 2023, American Physical Society.

cycloaddition. Unlike the nonconductive 2D C₆₀ polymer, 3D-P-27 is electron conductive. The success of synthesizing 3D SCPs under high-pressure conditions is a promising development, which opens up possibilities for the synthesis of other 3D SCPs using similar methods. Further research in this area is highly recommended to explore these possibilities.

5 Conclusions

The study of SCPs has emerged as a highly popular research subject over the past decade. The synthesis of such SCPs presents a challenging task for chemists, as they must exert complete control over the formation of chemical bonds as opposed to random polymerization. An atomic-level determination of atom positions, bond connections, and secondary interactions through single-crystal structure analysis can potentially offer solutions to many long-standing questions and concerns in polymeric architectures, including understanding polymerization mechanisms, controlling factors of structural orders, exploring potential applications based on their structures, and studying the physical properties of polymers.

Despite the potential benefits, the lack of general strategies to grow high-quality single crystals remains a significant challenge in SCPs synthesis. To date, solution synthesis and topochemical polymerization have been the primary strategies employed for the formation of SCPs. Although these methods offer great potential for the development of efficient and versatile SCP synthesis methods, both of these methods have limitations in terms of the choice of reaction types, and highly time-consuming trial-and-error experiments are unavoidable. Solution synthesis is highly dependent on imine-bond reactions, while topochemical polymerization is limited to irradiation- or heating-triggered reactions. Solution synthesis has the advantage of extending the topologies of the obtained structures, as the design of diversified monomers for structural diversity is much easier in this method. The polymerization kinetics are deemed to be critical based on the current understanding of solution synthesis. In contrast, topochemical polymerization is advantageous for the preparation of large-sized single crystals, as the size of the single-crystal monomers determines the size of the SCPs. Further studies in this area are highly encouraged to develop more efficient and versatile methods for the synthesis of SCPs.

The structure determination of the obtained SCPs at an atomic level is still limited to SCXRD and cRED. The cRED technique has become a well-accepted characterization technique for the structure determination of SCPs and will continue to play a key role in SCP materials. The cRED technique, although demanding in terms of technical expertise and optimization of operating conditions, requires smaller single crystals compared to SCXRD. However, it has not gained as much popularity as SCXRD for structure determination due to its technical demands. Moreover, successful applications of cRED to 2D SCPs are scarce, underscoring the importance of further investigation. Additionally, since both SCXRD and cRED demand high-quality single crystals, alternative techniques are

needed to determine the crystal structures of polycrystalline samples and circumvent the need for growing large single crystals. Any advancements in instrumentation and characterization techniques should be leveraged for the structure determination of SCPs. Cross-disciplinary approaches, such as cryo-transmission electron microscopy (cryo-TEM), are also encouraged to overcome existing limitations.

Advancements in the development of strategies to obtain SCPs are expected to significantly improve the structural diversity of SCPs, particularly 2D and 3D SCPs, realizing their full potential in the near future. These SCPs possess highly ordered structures, well-defined pores, and channels that offer unique characteristics, making them ideal for precise separation technology, nano-confinement catalysis, organic single-crystal devices, and many other applications. With an atomic-level determination of atom positions, bond connections, and secondary interactions through single-crystal structure analysis, researchers can gain insight into the structure-property relationship of these materials and reveal their intrinsic properties. Even though the application of SCPs has not been extensively studied, their immense potential is clear, and further research in this area is highly encouraged.

Author contributions

Y. Z and W. Z initiated the concept. M. W., Y. J., W. Z. and Y. Z. wrote the review together.

Conflicts of interest

There are no conflicts to declare.

Acknowledgements

This work was supported by the National Natural Science Foundation of China (22175101), the Natural Science Foundation of Shandong Province (ZR2020ZD38), and the National Science Foundation (CHE-2108197).

Notes and references

- 1 H. Staudinger, Ber. Dtsch. Chem. Ges., 1920, 53, 1073-1085.
- 2 H. Staudinger and J. Fritschi, Helv. Chim. Acta, 1922, 5, 785–806.
- 3 K. S. Novoselov, A. K. Geim, S. V. Morozov, D. Jiang, Y. Zhang, S. V. Dubonos, I. V. Grigorieva and A. A. Firsov, *Science*, 2004, **306**, 666–669.
- 4 P. Côté Adrien, I. Benin Annabelle, W. Ockwig Nathan, M. O'Keeffe, J. Matzger Adam and M. Yaghi Omar, *Science*, 2005, 310, 1166–1170.
- 5 M. El-Kaderi Hani, R. Hunt Joseph, L. Mendoza-Cortés José, P. Côté Adrien, E. Taylor Robert, M. O'Keeffe and M. Yaghi Omar, *Science*, 2007, 316, 268–272.
- 6 S. Diercks Christian and M. Yaghi Omar, *Science*, 2017, 355, eaal1585.

- 7 M. Xue, J. Yang, F. Kang, X. Wang and Q. Zhang, J. Mater. Chem. C, 2022, 10, 17027–17047.
- 8 B. Gui, H. Ding, Y. Cheng, A. Mal and C. Wang, *Trends Chem.*, 2022, **4**, 437–450.
- 9 M. J. Kory, M. Wörle, T. Weber, P. Payamyar, S. W. van de Poll, J. Dshemuchadse, N. Trapp and A. D. Schlüter, *Nat. Chem.*, 2014, **6**, 779–784.
- 10 D. Beaudoin, T. Maris and J. D. Wuest, *Nat. Chem.*, 2013, 5, 830–834.
- 11 T. Ma, A. Kapustin Eugene, X. Yin Shawn, L. Liang, Z. Zhou, J. Niu, L.-H. Li, Y. Wang, J. Su, J. Li, X. Wang, D. Wang Wei, W. Wang, J. Sun and M. Yaghi Omar, *Science*, 2018, 361, 48–52.
- 12 B. Gui, G. Lin, H. Ding, C. Gao, A. Mal and C. Wang, *Acc. Chem. Res.*, 2020, **53**, 2225–2234.
- 13 X. Guan, F. Chen, Q. Fang and S. Qiu, *Chem. Soc. Rev.*, 2020, 49, 1357–1384.
- 14 C. Gao, J. Li, S. Yin, G. Lin, T. Ma, Y. Meng, J. Sun and C. Wang, *Angew. Chem., Int. Ed.*, 2019, 58, 9770–9775.
- 15 W. Wan, J. Sun, J. Su, S. Hovmöller and X. Zou, *J. Appl. Crystallogr.*, 2013, **46**, 1863–1873.
- 16 Y.-B. Zhang, J. Su, H. Furukawa, Y. Yun, F. Gándara, A. Duong, X. Zou and O. M. Yaghi, J. Am. Chem. Soc., 2013, 135, 16336–16339.
- 17 P. H. Geil, J. Polym. Sci., 1960, 44, 449-458.
- 18 A. Keller, Polymer, 1962, 3, 393-421.
- 19 A. Keller, Kolloid Z. Z. Polym., 1969, 231, 386-421.
- 20 E. Martuscelli, J. Macromol. Sci., Part B, 1975, 11, 1-20.
- 21 R. H. Baughman, J. Polym. Sci.: Polym. Phys. Ed., 1974, 12, 1511–1535.
- 22 T. Okihara, M. Tsuji, A. Kawaguchi, K.-I. Katayama, H. Tsuji, S.-H. Hyon and Y. Ikada, *J. Macromol. Sci., Part B*, 1991, **30**, 119–140.
- 23 D. H. Kim, J. T. Han, Y. D. Park, Y. Jang, J. H. Cho, M. Hwang and K. Cho, *Adv. Mater.*, 2006, **18**, 719–723.
- 24 S. Z. D. Cheng, Nature, 2007, 448, 1006-1007.
- 25 H. Li and L. A. Estroff, Adv. Mater., 2009, 21, 470-473.
- 26 L. Cartier, T. Okihara and B. Lotz, *Macromolecules*, 1997, **30**, 6313–6322.
- 27 X. Liu, Y. Zhang, K. Goswami Dipak, S. Okasinski John, K. Salaita, P. Sun, J. Bedzyk Michael and A. Mirkin Chad, Science, 2005, 307, 1763–1766.
- 28 C. H. M. Weber, A. Chiche, G. Krausch, S. Rosenfeldt, M. Ballauff, L. Harnau, I. Göttker-Schnetmann, Q. Tong and S. Mecking, *Nano Lett.*, 2007, 7, 2024–2029.
- 29 B. Lotz, T. Miyoshi and S. Z. D. Cheng, *Macromol.*, 2017, 50, 5995–6025.
- 30 W. A. Henderson, N. R. Brooks and V. G. Young, *J. Am. Chem. Soc.*, 2003, **125**, 12098–12099.
- 31 C. Zhang, S. Gamble, D. Ainsworth, A. M. Z. Slawin, Y. G. Andreev and P. G. Bruce, *Nat. Mater.*, 2009, 8, 580–584.
- 32 A. J. Greenlee, C. I. Wendell, M. M. Cencer, S. D. Laffoon and J. S. Moore, *Trends Chem.*, 2020, **2**, 1043–1051.
- 33 A. Wilson, G. Gasparini and S. Matile, *Chem. Soc. Rev.*, 2014, **43**, 1948–1962.

34 D. Wang, L. Zhang and Y. Zhao, J. Org. Chem., 2022, 87, 2767-2772.

Chem Soc Rev

- 35 M. Mastalerz, Angew. Chem., Int. Ed., 2010, 49, 5042-5053.
- 36 Y. Jin, C. Yu, R. J. Denman and W. Zhang, Chem. Soc. Rev., 2013, 42, 6634-6654.
- 37 Y. Jin, Q. Wang, P. Taynton and W. Zhang, Acc. Chem. Res., 2014, 47, 1575-1586.
- 38 M. E. Belowich and J. F. Stoddart, Chem. Soc. Rev., 2012, 41, 2003-2024.
- 39 A. G. Orrillo and R. L. E. Furlan, Angew. Chem., Int. Ed., 2022, 61, e202201168.
- 40 F. Schaufelberger, B. J. J. Timmer and O. Ramström, in Dynamic Covalent Chemistry, ed. W. Zhang and Y. Jin, John Wiley & Sons, 2017, pp. 1-30, DOI: 10.1002/ 9781119075738.ch1.
- 41 T. Hasell and A. I. Cooper, Nat. Rev. Mater., 2016, 1, 16053.
- 42 W. Zhang and Y. Jin, Dynamic Covalent Chemistry: Principles, Reactions, and Applications, John Wiley & Sons, 2017.
- 43 S. Huang, Z. Lei, Y. Jin and W. Zhang, Chem. Sci., 2021, 12, 9591-9606.
- 44 X. Li, P. Yadav and K. P. Loh, Chem. Soc. Rev., 2020, 49, 4835-4866.
- 45 R. R. Liang, S. Y. Jiang, A. Ru-Han and X. Zhao, Chem. Soc. Rev., 2020, 49, 3920-3951.
- 46 Y. Jin, Y. Hu and W. Zhang, Nat. Rev. Chem., 2017, 1, 0056.
- 47 P. J. Waller, F. Gandara and O. M. Yaghi, Acc. Chem. Res., 2015, 48, 3053-3063.
- 48 K. Y. Geng, T. He, R. Y. Liu, S. Dalapati, K. T. Tan, Z. P. Li, S. S. Tao, Y. F. Gong, Q. H. Jiang and D. L. Jiang, Chem. Rev., 2020, 120, 8814-8933.
- 49 S. Y. Ding and W. Wang, Chem. Soc. Rev., 2013, 42, 548-568.
- 50 Y. S. Li, W. B. Chen, G. L. Xing, D. L. Jiang and L. Chen, Chem. Soc. Rev., 2020, 49, 2852-2868.
- 51 R. Y. Liu, K. T. Tan, Y. F. Gong, Y. Z. Chen, Z. E. Li, S. L. Xie, T. He, Z. Lu, H. Yang and D. L. Jiang, Chem. Soc. Rev., 2021, **50**, 120-242.
- 52 J. L. Segura, M. J. Mancheno and F. Zamora, Chem. Soc. Rev., 2016, 45, 5635-5671.
- 53 J. C. Jiang, Y. B. Zhao and O. M. Yaghi, J. Am. Chem. Soc., 2016, 138, 3255-3265.
- 54 S. Kandambeth, K. Dey and R. Banerjee, J. Am. Chem. Soc., 2019, 141, 1807-1822.
- 55 N. Huang, P. Wang and D. L. Jiang, Nat. Rev. Mater., 2016, 1, 16068.
- 56 H.-S. Xu, Y. Luo, X. Li, P. Z. See, Z. Chen, T. Ma, L. Liang, K. Leng, I. Abdelwahab, L. Wang, R. Li, X. Shi, Y. Zhou, X. F. Lu, X. Zhao, C. Liu, J. Sun and K. P. Loh, Nat. Commun., 2020, 11, 1434.
- 57 A. R. Navarro Jorge, Science, 2018, 361, 35.
- 58 Y. Hu, S. J. Teat, W. Gong, Z. Zhou, Y. Jin, H. Chen, J. Wu, Y. Cui, T. Jiang, X. Cheng and W. Zhang, Nat. Chem., 2021, 13, 660-665.
- 59 J. Atcher, P. Mateus, B. Kauffmann, F. Rosu, V. Maurizot and I. Huc, Angew. Chem., Int. Ed., 2021, 60, 2574-2577.
- 60 S. De, B. Chi, T. Granier, T. Qi, V. Maurizot and I. Huc, Nat. Chem., 2018, 10, 51-57.

- 61 Q. Gan, Y. Ferrand, C. Bao, B. Kauffmann, A. Grélard, H. Jiang and I. Huc, Science, 2011, 331, 1172-1175.
- 62 J. L. Greenfield, F. J. Rizzuto, I. Goldberga and J. R. Nitschke, Angew. Chem., Int. Ed., 2017, 56, 7541-7545.
- 63 H.-S. Xu, Y. Luo, P. Z. See, X. Li, Z. Chen, Y. Zhou, X. Zhao, K. Leng, I.-H. Park, R. Li, C. Liu, F. Chen, S. Xi, J. Sun and K. P. Loh, Angew. Chem., Int. Ed., 2020, 59, 11527-11532.
- 64 K. Tanaka and F. Toda, Chem. Rev., 2000, 100, 1025-1074.
- 65 K. Biradha and R. Santra, Chem. Soc. Rev., 2013, 42, 950-967.
- 66 X. Xiao, H. Wang, P. Urbankowski and Y. Gogotsi, Chem. Soc. Rev., 2018, 47, 8744-8765.
- 67 K. Hema, A. Ravi, C. Raju, J. R. Pathan, R. Rai and K. M. Sureshan, Chem. Soc. Rev., 2021, 50, 4062-4099.
- 68 K. Hema and K. M. Sureshan, Acc. Chem. Res., 2019, 52, 3149-3163.
- 69 J. W. Lauher, F. W. Fowler and N. S. Goroff, Acc. Chem. Res., 2008, 41, 1215-1229.
- 70 S.-L. Huang, T. S. A. Hor and G.-X. Jin, Coord. Chem. Rev., 2017, 346, 112-122.
- 71 T. Friščić and L. R. MacGillivray, Z. Med. Phys., 2005, 220, 351-363.
- 72 T. Devic, P. Batail and N. Avarvari, Chem. Commun., 2004, 1538-1539.
- 73 S. P. Yelgaonkar, G. Campillo-Alvarado and L. R. MacGillivray, J. Am. Chem. Soc., 2020, 142, 20772-20777.
- 74 Q. Chu, D. C. Swenson and L. R. MacGillivray, Angew. Chem., Int. Ed., 2005, 44, 3569-3572.
- 75 M. Garai, R. Santra and K. Biradha, Angew. Chem., Int. Ed., 2013, 52, 5548-5551.
- 76 H. A. Al-Mohsin, A. AlMousa, S. A. Oladepo, A. S. Jalilov, M. Fettouhi and A. M. P. Peedikakkal, *Inorg. Chem.*, 2019, 58, 10167-10173.
- 77 Q.-H. Guo, M. Jia, Z. Liu, Y. Qiu, H. Chen, D. Shen, X. Zhang, Q. Tu, M. R. Ryder, H. Chen, P. Li, Y. Xu, P. Li, Z. Chen, G. S. Shekhawat, V. P. Dravid, R. Q. Snurr, D. Philp, A. C. H. Sue, O. K. Farha, M. Rolandi and J. F. Stoddart, J. Am. Chem. Soc., 2020, 142, 6180-6187.
- 78 Q. Yu, M. Li, J. Gao, P. Xu, Q. Chen, D. Xing, J. Yan, M. J. Zaworotko, J. Xu, Y. Chen, P. Cheng and Z. Zhang, Angew. Chem., Int. Ed., 2019, 58, 18634-18640.
- 79 M. Servalli, N. Trapp and A. D. Schlüter, Chem. Eur. J., 2018, 24, 15003-15012.
- 80 P. Kissel, D. J. Murray, W. J. Wulftange, V. J. Catalano and B. T. King, Nat. Chem., 2014, 6, 774-778.
- 81 I. Turowska-Tyrk and E. Trzop, Acta Crystallogr. Sect. B, 2003, **59**, 779–786.
- 82 A. Matsumoto, T. Tanaka, T. Tsubouchi, K. Tashiro, S. Saragai and S. Nakamoto, J. Am. Chem. Soc., 2002, 124, 8891-8902.
- 83 T. Tanaka and A. Matsumoto, J. Am. Chem. Soc., 2002, 124, 9676-9677.
- 84 R. Samanta, D. Kitagawa, A. Mondal, M. Bhattacharya, M. Annadhasan, S. Mondal, R. Chandrasekar, S. Kobatake and C. M. Reddy, ACS Appl. Mater. Interfaces, 2020, 12, 16856-16863.
- 85 C. L. Anderson, H. Li, C. G. Jones, S. J. Teat, N. S. Settineri, E. A. Dailing, J. Liang, H. Mao, C. Yang, L. M. Klivansky,

- X. Li, J. A. Reimer, H. M. Nelson and Y. Liu, *Nat. Commun.*, 2021, **12**, 6818.
- 86 T. Itoh, S. Nomura, H. Nakasho, T. Uno, M. Kubo, N. Tohnai and M. Miyata, *Macromol.*, 2015, 48, 5450–5455.
- 87 T.-J. Hsu, F. W. Fowler and J. W. Lauher, *J. Am. Chem. Soc.*, 2012, **134**, 142–145.
- 88 J. J. Kane, R.-F. Liao, J. W. Lauher and F. W. Fowler, *J. Am. Chem. Soc.*, 1995, 117, 12003–12004.
- 89 P. Baillargeon, R. Robidas, C. Y. Legault, T. Rahem, A. Paré Fouapon and S.-M. Boivin, *Cryst. Growth Des.*, 2020, **20**, 5648–5656.
- 90 J. Xiao, M. Yang, J. W. Lauher and F. W. Fowler, *Angew. Chem.*, *Int. Ed.*, 2000, **39**, 2132–2135.
- 91 A. Sun, W. Lauher Joseph and S. Goroff Nancy, *Science*, 2006, 312, 1030–1034.
- 92 G. Wegner, Makromol. Chem., 1972, 154, 35-48.
- 93 V. Athiyarath and K. M. Sureshan, *Angew. Chem., Int. Ed.*, 2020, **59**, 15580–15585.
- 94 K. Hema and K. M. Sureshan, *Angew. Chem., Int. Ed.*, 2019, **58**, 2754–2759.
- 95 A. Pathigoolla and K. M. Sureshan, *Angew. Chem., Int. Ed.*, 2013, 52, 8671–8675.
- 96 A. Pathigoolla and K. M. Sureshan, *Angew. Chem., Int. Ed.*, 2014, 53, 9522–9525.
- 97 R. Mohanrao and K. M. Sureshan, *Angew. Chem., Int. Ed.*, 2018, 57, 12435–12439.
- 98 V. Athiyarath and K. M. Sureshan, *Angew. Chem., Int. Ed.*, 2019, **58**, 612–617.
- 99 V. Athiyarath, M. C. Madhusudhanan, S. Kunnikuruvan and K. M. Sureshan, *Angew. Chem., Int. Ed.*, 2022, **61**, e202113129.
- 100 W.-W. He, S.-L. Li and Y.-Q. Lan, *Inorg. Chem. Front.*, 2018, 5, 279–300.
- 101 A. Chaudhary, A. Mohammad and S. M. Mobin, *Cryst. Growth Des.*, 2017, **17**, 2893–2910.
- 102 F. Hu, X. Bi, X. Chen, Q. Pan and Y. Zhao, *Chem. Lett.*, 2021, **50**, 1015–1029.
- 103 M. Hasegawa, Y. Suzuki, F. Suzuki and H. Nakanishi, J. Polym. Sci., Part A-1: Polym. Chem., 1969, 7, 743–752.
- 104 V. Buchholz and V. Enkelmann, *Mol. Cryst. Liq. Cryst. Sci. Technol., Sect. A*, 2001, 356, 315–325.
- 105 K. Tashiro, H. Yamamoto, K. Sugimoto, T. Takahama, M. Tanaka and M. Hasegawa, *Macromolecules*, 2019, **52**, 2189–2202.
- 106 G. W. Coates, A. R. Dunn, L. M. Henling, J. W. Ziller, E. B. Lobkovsky and R. H. Grubbs, *J. Am. Chem. Soc.*, 1998, 120, 3641–3649.
- 107 R. Mandal, M. Garai and K. Biradha, *Cryst. Growth Des.*, 2017, **17**, 5061–5064.
- 108 R. Mandal, A. Garai, S. Peli, P. K. Datta and K. Biradha, Chem. - Eur. J., 2020, 26, 396-400.
- 109 P. Johnston, C. Braybrook and K. Saito, *Chem. Sci.*, 2012, 3, 2301–2306.
- 110 P. Johnston, D. Wheldale, C. Braybrook and K. Saito, *Polym. Chem.*, 2014, 5, 4375–4384.
- 111 Z. Wang, B. Kastern, K. Randazzo, A. Ugrinov, J. Butz, D. W. Seals, M. P. Sibi and Q. R. Chu, *Green Chem.*, 2015, 17, 4720–4724.

- 112 Z. Wang, B. Miller, J. Butz, K. Randazzo, Z. D. Wang and Q. R. Chu, *Angew. Chem., Int. Ed.*, 2017, **56**, 12155–12159.
- 113 Y. Liu, X.-R. Guan, D.-C. Wang, J. F. Stoddart and Q.-H. Guo, *J. Am. Chem. Soc.*, 2023, 145, 13223–13231.
- 114 S. Saragai, K. Tashiro, S. Nakamoto, T. Kamae, A. Matsumoto and T. Tsubouchi, *Polym. J.*, 2001, 33, 199–203.
- 115 A. Matsumoto, T. Odani, M. Chikada, K. Sada and M. Miyata, J. Am. Chem. Soc., 1999, 121, 11122–11129.
- 116 A. Matsumoto, T. Kunisue, S. Nagahama, A. Matsumoto, K. Sada, K. Inoue, T. Tanakaand and M. Miyata, *Mol. Cryst. Liq. Cryst.*, 2003, **390**, 11–18.
- 117 S. Nagahama and A. Matsumoto, *J. Am. Chem. Soc.*, 2001, 123, 12176-12181.
- 118 T. Odani, S. Okada, C. Kabuto, T. Kimura, S. Shimada, H. Matsuda, H. Oikawa, A. Matsumoto and H. Nakanishi, *Cryst. Growth Des.*, 2009, **9**, 3481–3487.
- 119 A. Matsumoto, D. Furukawa and H. Nakazawa, *J. Polym. Sci., Part A: Polym. Chem.*, 2006, 44, 4952–4965.
- 120 A. Matsumoto, T. Tanaka and K. Oka, *Synthesis*, 2005, 1479–1490.
- 121 A. Matsumoto, D. Furukawa, Y. Mori, T. Tanaka and K. Oka, *Cryst. Growth Des.*, 2007, 7, 1078–1085.
- 122 Y. Mori, T. Chiba, T. Odani and A. Matsumoto, *Cryst. Growth Des.*, 2007, 7, 1356–1364.
- 123 X. Hou, Z. Wang, J. Lee, E. Wysocki, C. Oian, J. Schlak and Q. R. Chu, *Chem. Commun.*, 2014, **50**, 1218–1220.
- 124 Y. Mori and A. Matsumoto, *Cryst. Growth Des.*, 2007, 7, 377–385.
- 125 A. Matsumoto, K. Sada, K. Tashiro, M. Miyata, T. Tsubouchi, T. Tanaka, T. Odani, S. Nagahama, T. Tanaka, K. Inoue, S. Saragai and S. Nakamoto, *Angew. Chem., Int. Ed.*, 2002, 41, 2502–2505.
- 126 L. Dou, Y. Zheng, X. Shen, G. Wu, K. Fields, W.-C. Hsu, H. Zhou, Y. Yang and F. Wudl, *Science*, 2014, 343, 272–277.
- 127 T. Hoang, J. W. Lauher and F. W. Fowler, *J. Am. Chem. Soc.*, 2002, **124**, 10656–10657.
- 128 T. Itoh, T. Suzuki, T. Uno, M. Kubo, N. Tohnai and M. Miyata, *Angew. Chem., Int. Ed.*, 2011, **50**, 2253–2256.
- 129 G. Wegner, Z. Naturforsch., 1969, 24, 824-832.
- 130 R. H. Baughman, J. Appl. Phys., 2003, 43, 4362-4370.
- 131 G. N. Patel, Radiat. Phys. Chem., 1981, 18, 913-925.
- 132 H. Tachibana, R. Kumai, N. Hosaka and Y. Tokura, *Chem. Mater.*, 2001, **13**, 155–158.
- 133 Y. L. Dory, M. Caron, V. O. Duguay, L. Chicoine-Ouellet, D. Fortin and P. Baillargeon, *Crystals*, 2019, **9**, 448.
- 134 H. Tabata, H. Tokoyama, H. Yamakado and T. Okuno, *J. Mater. Chem.*, 2012, **22**, 115–122.
- 135 T. Okuno, S. Ikeda, N. Kubo and D. J. Sandman, *Mol. Cryst. Liq. Cryst.*, 2006, **456**, 35–44.
- 136 S. Wang, Y. Li, H. Liu, J. Li, T. Li, Y. Wu, S. Okada and H. Nakanishi, *Org. Biomol. Chem.*, 2015, **13**, 5467–5474.
- 137 P. Tanphibal, K. Tashiro and S. Chirachanchai, *Macromol. Rapid Commun.*, 2016, 37, 685–690.
- 138 R. S. Jordan, Y. Wang, R. D. McCurdy, M. T. Yeung, K. L. Marsh, S. I. Khan, R. B. Kaner and Y. Rubin, *Chem*, 2016, 1, 78–90.

- 139 J. Deschamps, M. Balog, B. Boury, M. Ben Yahia, J.-S. Filhol, A. van der Lee, A. Al Choueiry, T. Barisien, L. Legrand, M. Schott and S. G. Dutremez, *Chem. Mater.*, 2010, 22, 3961–3982.
- 140 H. Tabata, K. Kuwamoto and T. Okuno, *J. Mol. Struct.*, 2016, **1106**, 452–459.
- 141 R. Xu, W. B. Schweizer and H. Frauenrath, *J. Am. Chem. Soc.*, 2008, **130**, 11437–11445.
- 142 R. Xu, V. Gramlich and H. Frauenrath, *J. Am. Chem. Soc.*, 2006, **128**, 5541–5547.
- 143 J. J. Kane, T. Nguyen, J. Xiao, F. W. Fowler and J. W. Lauher, *Mol. Cryst. Liq. Cryst. Sci. Technol., Sect. A*, 2001, 356, 449–458.
- 144 T. L. Nguyen, F. W. Fowler and J. W. Lauher, *J. Am. Chem. Soc.*, 2001, **123**, 11057–11064.
- 145 X. Ouyang, F. W. Fowler and J. W. Lauher, *J. Am. Chem. Soc.*, 2003, **125**, 12400–12401.
- 146 N. S. Goroff, S. M. Curtis, J. A. Webb, F. W. Fowler and J. W. Lauher, *Org. Lett.*, 2005, 7, 1891–1893.
- 147 L. Luo, C. Wilhelm, A. Sun, C. P. Grey, J. W. Lauher and N. S. Goroff, J. Am. Chem. Soc., 2008, 130, 7702–7709.
- 148 Z. Li, F. W. Fowler and J. W. Lauher, *J. Am. Chem. Soc.*, 2009, **131**, 634–643.
- 149 A. Matsumoto, A. Matsumoto, T. Kunisue, A. Tanaka, N. Tohnai, K. Sada and M. Miyata, *Chem. Lett.*, 2003, 33, 96–97.
- 150 A. Sun, J. W. Lauher and N. S. Goroff, *Science*, 2006, **312**, 1030–1034.
- 151 R. Khazeber and K. M. Sureshan, *Angew. Chem., Int. Ed.*, 2021, **60**, 24875–24881.
- 152 A. Ravi, A. Shijad and K. M. Sureshan, *Chem. Sci.*, 2021, **12**, 11652–11658.
- 153 R. Khazeber and K. M. Sureshan, *Proc. Natl. Acad. Sci. U. S. A.*, 2022, **119**, e2205320119.
- 154 V. Athiyarath, L. A. Mathew, Y. Zhao, R. Khazeber, U. Ramamurty and K. M. Sureshan, *Chem. Sci.*, 2023, 14, 5132–5140.
- 155 C. Raju, G. R. Ramteke, K. V. J. Jose and K. M. Sureshan, *J. Am. Chem. Soc.*, 2023, **145**, 9607–9616.
- 156 S. Bhandary, A. Pathigoolla, M. C. Madhusudhanan and K. M. Sureshan, *Chem. Eur. J.*, 2022, **28**, e202200820.
- 157 K. Hema and K. M. Sureshan, *Angew. Chem., Int. Ed.*, 2020, 59, 8854–8859.
- 158 R. Mohanrao, K. Hema and K. M. Sureshan, *Nat. Commun.*, 2020, **11**, 865.
- 159 K. Wang, D. D. Qi, Y. L. Li, T. Y. Wang, H. B. Liu and J. Z. Jiang, *Coord. Chem. Rev.*, 2019, 378, 188–206.
- 160 R.-B. Lin, Y. He, P. Li, H. Wang, W. Zhou and B. Chen, Chem. Soc. Rev., 2019, 48, 1362–1389.
- 161 H. Li, M. Eddaoudi, M. O'Keeffe and O. M. Yaghi, *Nature*, 1999, **402**, 276–279.
- 162 L. E. Kreno, K. Leong, O. K. Farha, M. Allendorf, R. P. Van Duyne and J. T. Hupp, *Chem. Rev.*, 2012, **112**, 1105–1125.
- 163 N. Stock and S. Biswas, Chem. Rev., 2012, 112, 933-969.
- 164 S. Horike, S. Shimomura and S. Kitagawa, *Nat. Chem.*, 2009, **1**, 695–704.

- 165 H. C. Zhou and S. Kitagawa, Chem. Soc. Rev., 2014, 43, 5415–5418.
- 166 M. Kondo, T. Yoshitomi, H. Matsuzaka, S. Kitagawa and K. Seki, Angew. Chem., Int. Ed. Engl., 1997, 36, 1725–1727.
- 167 C. Gropp, T. Ma, N. Hanikel and M. Yaghi Omar, *Science*, 2020, **370**, eabd6406.
- 168 M. Evans Austin, R. Parent Lucas, C. Flanders Nathan, P. Bisbey Ryan, E. Vitaku, S. Kirschner Matthew, D. Schaller Richard, X. Chen Lin, C. Gianneschi Nathan and R. Dichtel William, *Science*, 2018, 361, 52–57.
- 169 A. Natraj, W. Ji, J. Xin, I. Castano, D. W. Burke, A. M. Evans, M. J. Strauss, M. Ateia, L. S. Hamachi, N. C. Gianneschi, Z. A. Alothman, J. Sun, K. Yusuf and W. R. Dichtel, *J. Am. Chem. Soc.*, 2022, 144, 19813–19824.
- 170 C. Kang, K. Yang, Z. Zhang, A. K. Usadi, D. C. Calabro, L. S. Baugh, Y. Wang, J. Jiang, X. Zou, Z. Huang and D. Zhao, *Nat. Commun.*, 2022, **13**, 1370.
- 171 S. Patwardhan, A. A. Kocherzhenko, F. C. Grozema and L. D. A. Siebbeles, *J. Phys. Chem. C*, 2011, 115, 11768–11772.
- 172 F. Auras, L. Ascherl, A. H. Hakimioun, J. T. Margraf,
 F. C. Hanusch, S. Reuter, D. Bessinger, M. Döblinger,
 C. Hettstedt, K. Karaghiosoff, S. Herbert, P. Knochel,
 T. Clark and T. Bein, J. Am. Chem. Soc., 2016, 138, 16703–16710.
- 173 J. Sakamoto, J. van Heijst, O. Lukin and A. D. Schlüter, *Angew. Chem., Int. Ed.*, 2009, **48**, 1030–1069.
- 174 R. Z. Lange, G. Hofer, T. Weber and A. D. Schlüter, *J. Am. Chem. Soc.*, 2017, **139**, 2053–2059.
- 175 G. M. J. Schmidt, Pure Appl. Chem., 1971, 27, 647-678.
- 176 F. Hu, W. Hao, D. Mücke, Q. Pan, Z. Li, H. Qi and Y. Zhao, *J. Am. Chem. Soc.*, 2021, **143**, 5636–5642.
- 177 X. Jiang, X. Cui, A. J. E. Duncan, L. Li, R. P. Hughes, R. J. Staples, E. V. Alexandrov, D. M. Proserpio, Y. Wu and C. Ke, *J. Am. Chem. Soc.*, 2019, 141, 10915–10923.
- 178 Y. He, S. Xiang and B. Chen, *J. Am. Chem. Soc.*, 2011, **133**, 14570–14573.
- 179 R. Liang, J. Samanta, B. Shao, M. Zhang, R. J. Staples, A. D. Chen, M. Tang, Y. Wu, I. Aprahamian and C. Ke, *Angew. Chem., Int. Ed.*, 2021, **60**, 23176–23181.
- 180 J. Samanta, R. W. Dorn, W. Zhang, X. Jiang, M. Zhang, R. J. Staples, A. J. Rossini and C. Ke, *Chem*, 2022, 8, 253–267.
- 181 R. Z. Lange, K. Synnatschke, H. Qi, N. Huber, G. Hofer, B. Liang, C. Huck, A. Pucci, U. Kaiser, C. Backes and A. D. Schlüter, *Angew. Chem., Int. Ed.*, 2020, 59, 5683–5695.
- 182 J. Dong, L. Liu, C. Tan, Q. Xu, J. Zhang, Z. Qiao, D. Chu, Y. Liu, Q. Zhang, J. Jiang, Y. Han, A. P. Davis and Y. Cui, *Nature*, 2022, 602, 606–611.
- 183 D. W. Burke, C. Sun, I. Castano, N. C. Flanders, A. M. Evans, E. Vitaku, D. C. McLeod, R. H. Lambeth, L. X. Chen, N. C. Gianneschi and W. R. Dichtel, *Angew. Chem., Int. Ed.*, 2020, 59, 5165–5171.
- 184 X. D. Chen, Y. S. Li, L. Wang, Y. Xu, A. M. Nie, Q. Q. O. Li, F. Wu, W. W. Sun, X. Zhang, R. Vajtai, P. M. Ajayan, L. Chen and Y. Wang, Adv. Mater., 2019, 31, 1901640.

185 G. Das, B. P. Biswal, S. Kandambeth, V. Venkatesh, G. Kaur, M. Addicoat, T. Heine, S. Verma and R. Banerjee, *Chem. Sci.*, 2015, **6**, 3931–3939.

Review Article

- 186 J. Q. Dong, X. Li, S. B. Peh, Y. D. Yuan, Y. X. Wang, D. X. Ji, S. J. Peng, G. L. Liu, S. M. Ying, D. Q. Yuan, J. W. Jiang, S. Ramakrishna and D. Zhao, *Chem. Mater.*, 2019, 31, 146–160.
- 187 D. Rodriguez-San-Miguel, C. Montoro and F. Zamora, *Chem. Soc. Rev.*, 2020, **49**, 2291–2302.
- 188 S. Wang, Q. Y. Wang, P. P. Shao, Y. Z. Han, X. Gao, L. Ma, S. Yuan, X. J. Ma, J. W. Zhou, X. Feng and B. Wang, *J. Am. Chem. Soc.*, 2017, 139, 4258–4261.
- 189 V. Müller, F. Shao, M. Baljozovic, M. Moradi, Y. Zhang, T. Jung, W. B. Thompson, B. T. King, R. Zenobi and A. D. Schlüter, Angew. Chem., Int. Ed., 2017, 56, 15262–15266.
- 190 W. Dai, F. Shao, J. Szczerbiński, R. McCaffrey, R. Zenobi, Y. Jin, A. D. Schlüter and W. Zhang, *Angew. Chem., Int. Ed.*, 2016, 55, 213–217.
- 191 V. Müller, A. Hinaut, M. Moradi, M. Baljozovic, T. A. Jung, P. Shahgaldian, H. Möhwald, G. Hofer, M. Kröger, B. T. King, E. Meyer, T. Glatzel and A. D. Schlüter, *Angew. Chem., Int. Ed.*, 2018, 57, 10584–10588.
- 192 K. Liu, H. Qi, R. Dong, R. Shivhare, M. Addicoat, T. Zhang,
 H. Sahabudeen, T. Heine, S. Mannsfeld, U. Kaiser,
 Z. Zheng and X. Feng, *Nat. Chem.*, 2019, 11, 994–1000.
- 193 R. H. Dong, T. Zhang and X. L. Feng, Chem. Rev., 2018, 118, 6189–6235.
- T. Zhang, H. Qi, Z. Liao, Y. D. Horev, L. A. Panes-Ruiz,
 P. S. Petkov, Z. Zhang, R. Shivhare, P. Zhang, K. Liu,
 V. Bezugly, S. Liu, Z. Zheng, S. Mannsfeld, T. Heine,
 G. Cuniberti, H. Haick, E. Zschech, U. Kaiser, R. Dong and X. Feng, Nat. Commun., 2019, 10, 4225.
- 195 H. Sahabudeen, H. Qi, M. Ballabio, M. Položij, S. Olthof, R. Shivhare, Y. Jing, S. Park, K. Liu, T. Zhang, J. Ma, B. Rellinghaus, S. Mannsfeld, T. Heine, M. Bonn, E. Cánovas, Z. Zheng, U. Kaiser, R. Dong and X. Feng, Angew. Chem., Int. Ed., 2020, 59, 6028–6036.
- 196 Z. Zhang, C. Wu, Q. Pan, F. Shao, Q. Sun, S. Chen, Z. Li and Y. Zhao, *Chem. Commun.*, 2020, **56**, 3210–3213.
- 197 Q. Sun, Q. Pan, Y. Ban, H. Liu, C. Fan, L. Sun and Y. Zhao, *Chem. Eur. J.*, 2021, 27, 3661–3664.
- 198 H. Sahabudeen, H. Y. Qi, B. A. Glatz, D. Tranca, R. H. Dong, Y. Hou, T. Zhang, C. Kuttner, T. Lehnert, G. Seifert, U. Kaiser, A. Fery, Z. K. Zheng and X. L. Feng, Nat. Commun., 2016, 7, 13461.
- 199 F. L. Tan, S. Han, D. L. Peng, H. L. Wang, J. Yang, P. Zhao,
 X. J. Ye, X. Dong, Y. Y. Zheng, N. Zheng, L. Gong,
 C. L. Liang, N. Frese, A. Golzhauser, H. Y. Qi, S. S. Chen,
 W. Liu and Z. K. Zheng, *J. Am. Chem. Soc.*, 2021, 143, 3927–3933.
- 200 R. Matsuoka, R. Sakamoto, K. Hoshiko, S. Sasaki, H. Masunaga, K. Nagashio and H. Nishihara, J. Am. Chem. Soc., 2017, 139, 3145–3152.
- 201 K. Dey, M. Pal, K. C. Rout, H. S. Kunjattu, A. Das, R. Mukherjee, U. K. Kharul and R. Banerjee, *J. Am. Chem. Soc.*, 2017, **139**, 13083–13091.

- 202 M. Matsumoto, L. Valentino, G. M. Stiehl, H. B. Balch, A. R. Corcos, F. Wang, D. C. Ralph, B. J. Marinas and W. R. Dichtel, *Chem*, 2018, 4, 308–317.
- 203 D. Zhou, X. Y. Tan, H. M. Wu, L. H. Tian and M. Li, Angew. Chem., Int. Ed., 2019, 58, 1376–1381.
- 204 X. L. Feng and A. D. Schluter, *Angew. Chem., Int. Ed.*, 2018, 57, 13748–13763.
- 205 Y. Jin, Y. Hu, M. Ortiz, S. Huang, Y. Ge and W. Zhang, *Chem. Soc. Rev.*, 2020, **49**, 4637–4666.
- 206 X. Chen, S. Yamanaka, K. Sako, Y. Inoue and M. Yasukawa, *Chem. Phys. Lett.*, 2002, **356**, 291–297.
- 207 M. Núñez-Regueiro, L. Marques, J. L. Hodeau, O. Béthoux and M. Perroux, *Phys. Rev. Lett.*, 1995, 74, 278–281.
- 208 S. Yamanaka, A. Kubo, K. Inumaru, K. Komaguchi, N. S. Kini, T. Inoue and T. Irifune, *Phys. Rev. Lett.*, 2006, 96, 076602.
- 209 X. Chen and S. Yamanaka, Chem. Phys. Lett., 2002, 360, 501-508.
- 210 V. D. Blank, S. G. Buga, G. A. Dubitsky, N. R. Serebryanaya, M. Y. Popov and B. Sundqvist, *Carbon*, 1998, 36, 319–343.
- 211 Y. Iwasa, T. Arima, R. M. Fleming, T. Siegrist, O. Zhou, R. C. Haddon, L. J. Rothberg, K. B. Lyons, H. L. Carter, A. F. Hebard, R. Tycko, G. Dabbagh, J. J. Krajewski, G. A. Thomas and T. Yagi, *Science*, 1994, 264, 1570–1572.
- 212 S. Margadonna, D. Pontiroli, M. Belli, T. Shiroka, M. Riccò and M. Brunelli, *J. Am. Chem. Soc.*, 2004, **126**, 15032–15033.
- 213 P. W. Stephens, G. Bortel, G. Faigel, M. Tegze, A. Jánossy, S. Pekker, G. Oszlanyi and L. Forró, *Nature*, 1994, 370, 636–639.
- 214 A. F. Hebard, M. J. Rosseinsky, R. C. Haddon, D. W. Murphy, S. H. Glarum, T. T. M. Palstra, A. P. Ramirez and A. R. Kortan, *Nature*, 1991, 350, 600-601.
- 215 M. J. Rosseinsky, A. P. Ramirez, S. H. Glarum, D. W. Murphy, R. C. Haddon, A. F. Hebard, T. T. M. Palstra, A. R. Kortan, S. M. Zahurak and A. V. Makhija, *Phys. Rev. Lett.*, 1991, 66, 2830–2832.
- 216 S. Margadonna and K. Prassides, *J. Solid State Chem.*, 2002, **168**, 639–652.
- 217 L. Forró and L. Mihály, Rep. Prog. Phys., 2001, 64, 649-699.
- 218 R. P. Gupta and M. Gupta, Phys. C, 1994, 219, 21-25.
- 219 D. W. Murphy, M. J. Rosseinsky, R. M. Fleming, R. Tycko, A. P. Ramirez, R. C. Haddon, T. Siegrist, G. Dabbagh, J. C. Tully and R. E. Walstedt, *J. Phys. Chem. Solids*, 1992, 53, 1321–1332.
- 220 M. Tanaka and S. Yamanaka, *Cryst. Growth Des.*, 2018, 18, 3877–3882.
- 221 L. Hou, X. Cui, B. Guan, S. Wang, R. Li, Y. Liu, D. Zhu and J. Zheng, *Nature*, 2022, **606**, 507–510.
- 222 L. Liang, Y. Qiu, W. D. Wang, J. Han, Y. Luo, W. Yu, G.-L. Yin, Z.-P. Wang, L. Zhang, J. Ni, J. Niu, J. Sun, T. Ma and W. Wang, *Angew. Chem., Int. Ed.*, 2020, 59, 17991–17995.
- 223 C. Gao, J. Li, S. Yin, J. Sun and C. Wang, *J. Am. Chem. Soc.*, 2020, **142**, 3718–3723.
- 224 X. Liu, J. Li, B. Gui, G. Lin, Q. Fu, S. Yin, X. Liu, J. Sun and C. Wang, *J. Am. Chem. Soc.*, 2021, **143**, 2123–2129.
- 225 Y. Xie, J. Li, C. Lin, B. Gui, C. Ji, D. Yuan, J. Sun and C. Wang, *J. Am. Chem. Soc.*, 2021, **143**, 7279–7284.

- 226 C. Gao, J. Li, S. Yin, J. Sun and C. Wang, Nat. Commun., 2020, 11, 4919.
- 227 Y. Liu, P. Chen, Y. Wang, J. Suo, J. Ding, L. Zhu, V. Valtchev, Y. Yan, S. Qiu, J. Sun and Q. Fang, Angew. Chem., Int. Ed., 2022, 61, e202203584.
- 228 F. Jin, E. Lin, T. Wang, S. Geng, L. Hao, Q. Zhu, Z. Wang, Y. Chen, P. Cheng and Z. Zhang, J. Am. Chem. Soc., 2022, 144, 23081-23088.
- 229 Z. Zhou, L. Zhang, Y. Yang, I. J. Vitorica-Yrezabal, H. Wang, F. Tan, L. Gong, Y. Li, P. Chen, X. Dong, Z. Liang, J. Yang, C. Wang, Y. Hong, Y. Qiu, A. Gölzhäuser, X. Chen, H. Qi, S. Yang, W. Liu, J. Sun and Z. Zheng, Nat. Chem., 2023, 15, 841-847.
- 230 Y. Liu, Y. Ma, Y. Zhao, X. Sun, F. Gándara, H. Furukawa, Z. Liu, H. Zhu, C. Zhu, K. Suenaga, P. Oleynikov, S. Alshammari Ahmad, X. Zhang, O. Terasaki and M. Yaghi Omar, Science, 2016, 351, 365-369.
- 231 Y. Zhao, L. Guo, F. Gándara, Y. Ma, Z. Liu, C. Zhu, H. Lyu, C. A. Trickett, E. A. Kapustin, O. Terasaki and O. M. Yaghi, J. Am. Chem. Soc., 2017, 139, 13166-13172.
- 232 Y. Liu, Y. Ma, J. Yang, C. S. Diercks, N. Tamura, F. Jin and O. M. Yaghi, J. Am. Chem. Soc., 2018, 140, 16015-16019.
- 233 Y. Liu, C. S. Diercks, Y. Ma, H. Lyu, C. Zhu, S. A. Alshmimri, S. Alshihri and O. M. Yaghi, J. Am. Chem. Soc., 2019, 141, 677-683.
- 234 C. Sun, J. J. Oppenheim, G. Skorupskii, L. Yang and M. Dincă, Chem, 2022, 8, 3215-3224.